Experimental investigation of high-power continuous-wave fiber optical parametric amplifiers and oscillators.

Malik, Rohit

Experimental Investigation of High-Power Continuous-Wave Fiber Optical Parametric Amplifiers and Oscillators

Swansea University
Prifysgol Abertawe

by

Rohit Malik

Submitted in Partial Fulfilment
of the
Requirements for the Degree
Doctor of Philosophy

Supervised by

Prof. Michel E Marhic

College of Engineering, Swansea University

Swansea, SA2 8PP

United Kingdom

2010.

Abstract

Fiber optical parametric amplifiers (OPAs) are based on a highly-efficient four-wave mixing process. Their capability to give very high gain and large bandwidths have made them an attractive candidate for providing higher bandwidths for future telecommunication systems, such as wavelength-division multiplexed (WDM) photonics networks. In dynamic photonic networks a where number of channels are dropped and/or added all the time, the OPA gain for the other channels is affected. In this thesis we employed a well-known gain control technique, all-optical gain clamping (AOGC), and reduced the gain variation of fiber OPAs below 0.5 dB, under varying input conditions. We also showed an improvement in power penalties at the bit-error rate of 10^{-8}, from 2.5 dB to 0.5 dB for on/off keying modulation.

We also investigated fiber optical parametric oscillators (OPOs). Using fiber OPAs as gain medium we realized two different continuous-wave (CW) OPOs, centred at 1561 nm and 1593 nm. One gave us watt-level output power from 1600 nm to 1670 nm, with overall tuning range of 211 nm. The output linewidth of signal and idler was measured to be 0.08 nm and 0.15 nm respectively. The OPO centred at 1593 nm gave us a record tuning range of 254 nm, and with 3 dB output coupling fraction, it gave us large output powers (20-27 dBm) from 1610 nm to 1720 nm.

Using a large seed generated by a watt-level fiber OPO in the U-band, and using 3 W of CW pump source in the C-band for Raman amplification, we generated 3 W of CW output power. This gave us nearly 100% conversion efficiency.

Launching a high-power CW pump with narrow linewidth into a fiber makes stimulated Brillouin scattering (SBS) a major problem. We investigated an SBS suppressor, based on a common technique of phase dithering of the pump to suppress the SBS. We compared a multitone modulation technique to modulation with a pseudo-random bit sequence (PRBS), and we showed that it can increase the SBS threshold by 4.18 dB, and is less expensive to implement.

List of Publications:

[A] **R. Malik** and M. E. Marhic, "Gain Clamping in a Fiber Optical Parametric Amplifier," in *Optical Fiber Communication Conference*, OSA Technical Digest (CD) (Optical Society of America, 2010), paper JWA17.

[B] **R. Malik** and M. E. Marhic, "Reduction of Cross-Gain Modulation in a Fiber Optical Parametric Amplifier by Using All-Optical Gain Clamping," in *Latin America Optics and Photonics Conference*, OSA Technical Digest (CD) (Optical Society of America, 2010), paper PDPTuK3.

[C] **R. Malik** and M.E.Marhic, "Reduction of Cross-Gain Modulation in a Fiber Optical Parametric Amplifier by Using All-Optical Gain Clamping," submitted to *Photon. Techno. Lett.*

[D] **R. Malik** and M. E. Marhic, "Tunable Continuous-Wave Fiber Optical Parametric Oscillator with 1-W Output Power," in *Optical Fiber Communication Conference*, OSA Technical Digest (CD) (Optical Society of America, 2010), paper JWA18.

[E] **R. Malik** and M.E.Marhic, "Narrow-Linewidth Tunable Continuous-Wave Fiber Optical Parametric Oscillator with 1 W Output Power," in ECOC 2010, 19-23 September 2010, Turin, Italy, paper Th.10.C.5.

[F] **R. Malik** and M. E. Marhic, "Continuous Wave Fiber Optical Parametric Oscillator with 254 nm Tuning Range," in *Latin America Optics and Photonics Conference*, OSA Technical Digest (CD) (Optical Society of America, 2010), paper MD1.

[G] **R. Malik** and M.E.Marhic, "High-Power Continuous-Wave Fiber Optical Parametric Oscillators," *To be published in Nova press.*

[H] **R. Malik** and M.E.Marhic, "Tunable U-Band Raman Fiber Source with 3 W CW Output Power," in *IEEE Photonics Society Summer Topicals,* 19-21 July 2010, Playadel Carmen, Mexico, paper MC4.2

[I] **R.Malik** and M.E.Marhic, "Comparison of multi-tone and PRBS RF modulation for SBS suppression in optical fibers," in *International conference on Fiber Optics and Photonics,* December 13-17, 2010, New Delhi, India, paper PM-56.

DECLARATION

This work has not previously been accepted in substance for any degree and is not being concurrently submitted in candidature for any degree.

Signed ..... (candidate)

Date 17/12/2010

STATEMENT 1

This thesis is the result of my own investigations, except where otherwise stated. Where correction services have been used, the extent and nature of the correction is clearly marked in the footnote(s).

Other sources are acknowledged by footnotes giving explicit references. A bibliography is appended at the end of each chapter.

Signed ..... (candidate)

Date 17/12/2010

STATEMENT 2

I hereby give consent for my thesis, if accepted, to be available for photocopying and for inter-library loan, and for the title and summary to be made available to outside organisations.

Signed ..... (candidate)

Date 17/12/2010

Dedicated to My Parents

(Onkar Singh Malik and Saroj Malik)

Table of Contents

Acknowledgement

"If you shut the door to all errors, truth will be shut out".

Rabindranath Tagore

My acknowledgments are due to all the people who have influenced my life and have given me their blessings and support. I came to Swansea with a background in theoretical Physics and little experimental knowledge, but the tremendous support from everyone I worked here with made it possible for me to reach this far. The study was contributed my many helping hands without which it would have been a mammoth task. There are too many people to mention individually, but some names stand out. I'm grateful to my supervisor Prof. Michel E Marhic for taking me as a student and guiding me in every way I could think of. He has been more than a mentor to me throughout the study and his immense influence on my work can be felt everywhere in the thesis. I'm thankful to him for his invaluable support, encouragement and freedom. I am deeply indebted to him for the time and patience that he invested in every aspect of my doctoral research. This work certainly owes more to him than anyone else.

I also want to thank the other members of our laboratory whom I worked with, namely Dr. Hong Lu, Dr. Per Kylemark, Dr. Armand Vedadi, and Mehdi Jamshidifar. I earnestly thank Dr. Donald Govan, Dr Nayla El-Dahdah and Marcelo Zannin da Rosa for their helpful suggestions. A vote of thanks also goes to Mr. John Davies for providing me technical parts needed for my research, and Mrs Anjana Choudhury for helping me in the administrative part.

A very special thanks goes to my family which is 6,136 miles (thanks to Google Map) away from me. They haven't seen me for 2 years now but keep giving me their support and encouragement. And I dedicate this thesis to my family.

I also thank my friends Prafulla Deo, Arpan Pal, Anna Flicker, Robert Bevan and Stanislav Zapryanov here in Swansea; Daksh Panwar, Amitesh Mishra, Vibhor Singh, and Kaushik Choudhury in India; and Arun Sehrawat in Singapore, for boosting my morale and helping me stay positive. And for those who contributed in one way or the other but whose names are not mentioned here, you are not forgotten.

List of Tables

List of Figures

Abbreviations used in the text

OPA	Optical Parametric Amplifier
OPO	Optical Parametric Oscillator
BER	Bit-error rate
EDFA	Erbium Doped Fiber Amplifier
TL	Tunable Laser
OOK	On/Off Keyed
XGM	Cross-Gain Modulation
SBS	Stimulated Brillouin Scattering
RA	Raman Amplification
AOGC	All-Optical Gain-Clamping
PM	Phase Modulator
PC	Polarization Controller
TBPF	Tunable Band-Pass Filter
ASE	Amplified Spontaneous Emission
WDM	Wavelength Division Multiplexing
PRBS	Psuedo Random Bit-Sequence
FWM	Four-wave Mixing
VOA	Variable Optical Attenuator
CW	Continuous-Wave
SOP	State of Polarization
HNLF	Highly Nonlinear Fiber
ZDWL	Zero-dispersion Wavelength
DSF	Dispersion Shifted Fiber

Chapter 1

Introduction

Nonlinear optics was first investigated in 1961, soon after the first laser demonstration was made in 1960 [1.1]. Both parametric amplification and oscillation soon followed [1.2][1.3][1.4]. An optical parametric amplifier (OPA) amplifies a signal by using the nonlinearity of the medium and a strong pump wave (or two). The nonlinearity can be of two types: second order (χ^2) or third order (χ^3). In media with centrosymmetries such as optical fibers, χ^2 is not present, and χ^3 is responsible for most of the nonlinear effects. The χ^2 nonlinearity occurs mostly in crystals, such as periodically-poled Lithium Niobate (PPLN), Potassium Titanyl Phosphate (KTP), BBO, etc.

The χ^2 nonlinearity is responsible for effects such as second harmonic generation (SHG), difference and sum frequency generation (DFG and SFG). The χ^3 nonlinearity is responsible for effects such as four-wave mixing (FWM), stimulated Brillouin scattering (SBS), stimulated Raman scattering (SRS), self-phase modulation (SPM), cross-phase modulation (XPM), etc.

After several decades of development, parametric amplification in χ^3 media has come a long way. It can now provide several hundred nanometres of gain bandwidth and very high conversion efficiency [1.5]. Other types of optical amplifiers such as Erbium-doped fiber amplifiers (EDFAs), and semiconductor optical amplifiers (SOAs) have already been available commercially for many years. But EDFAs provide a typical bandwidth of only about 35 nm.

The ever-increasing number of Internet users, and the growing popularity of new services such as high-definition television (HDTV), YouTube, etc. requires more and more bandwidth. Fiber optical parametric amplifiers (OPAs) can provide hundreds of nanometres of bandwidth [1.5][1.6]. So fiber OPAs could prove an apt match for the future requirements of wideband photonic networks.

To have a large amount of information propagating through a fiber, several signals need to propagate together, on different optical carriers. This is known as wavelength division multiplexing (WDM). Although photons, unlike electrons, are considered to not interact with each other, this does not hold true when they travel in a fiber over a sufficiently long distance. Then they can interact via cross-phase modulation (XPM), cross-gain modulation (XGM), etc. These give rise to nonlinear crosstalk, which may degrade the quality of the signals. Since fiber OPAs are based on the use of nonlinear fibers, they are prone to generate such nonlinear crosstalk. This is one of the drawbacks of using fiber OPAs in photonic networks.

Different studies have been performed to reduce such crosstalk. To reduce FWM, the spacing between the channels could be uneven [1.7]. To reduce XGM, differential phase shift keying (DPSK) modulation could be used [1.8]. In this respect, Kuo et al. showed that DPSK modulation improves power penalties over on/off keying from 2.5 dB to 1.5 dB. But this study holds valid only under steady traffic conditions. However, as the demand for bandwidth increases, users also require dynamically-reconfigurable optical network architectures. In such networks, the input conditions such as number of input channels, input power per channel, etc. may vary with time, and fiber OPAs behave differently than under steady conditions. Part of this research is to study the behaviour of fiber OPAs under varying input conditions. To counteract the issues which arise, we have investigated all-optical

gain clamping (AOGC), which can control the gain of a fiber OPA under varying input conditions [A][B][C].

The architecture of an OPA with AOGC consists of an OPA with a feedback from output to input, which leads to laser oscillation, in a spectral region removed from the signal. So in effect an OPA with AOGC is actually also an optical parametric oscillator, or OPO. Because of the close relationship between an OPA with AOGC and an OPO, we have also undertaken the investigation of the properties of several types of fiber OPOs.

OPOs based on χ^2 materials were first observed in early 60s. At present they are commercially available. They can provide enormous amounts of tuning range, from 500 nm to 7000 nm. The threshold for these OPOs is relatively high (a few watts), so they are mostly pumped by pulsed pumps.

By contrast, the development of fiber OPOs has been much slower. This was due in part to the lack of availability of high-power CW pumps. Also, commercially available low-loss fibers had low nonlinearity coefficients. But in the last decade or so highly-nonlinear fibers (HNLFs) have become available. They have a nonlinearity coefficient an order of magnitude higher than that of standard single mode fiber (SSMF). Also with the availability of high output power EDFAs, it has become feasible to launch several watts of CW pump power into the fibers. This has spurred the interest into CW fiber OPOs. Part of this research involves making high output power (watt-level) and ultra-large tuning ranges (>200 nm) CW fiber OPOs [D][E][F][G], which are made possible by the availability of HNLFs and multi-watt pump powers.

Another χ^3 amplification mechanism that depends on the nonlinearity of the medium is Raman amplification. An important feature of Raman amplification is that by choosing a suitable pump wavelength, gain can be obtained in desired wavelength regions. Part of the thesis research involves the design and testing of a high output power source in the U-band (around 1650 nm) using fiber Raman amplification of a strong seed generated by a fiber OPO [G][H].

Apart from being a boon, fiber nonlinearity can also be a hindrance at times. For instance back-reflecting stimulated Brillouin scattering (SBS) is a major problem for the launching narrow linewidth CW pump power into the fibers [1.9][1.10]. Specifically, SBS puts a limit on the amount of power that we can launch into a fiber, if a narrow-linewidth pump is used. For this reason, we have also investigated techniques for reducing SBS. There are several techniques to counteract this problem, such as phase/frequency dithering of the pump [1.11][1.12], or creating a strain distribution along the fiber [1.13], and using temperature variations along the fiber [1.14]. Phase dithering is the most commonly used technique. Different RF sources such as pseudo-random bit sequence (PRBS), multi-tone RF phase modulation, etc. We have designed and built a multi-tone RF phase modulator and compared it with the PRBS in terms of SBS threshold increase, and price [I].

The thesis is organized as follows:

In Chapter 2, we introduce the fiber OPA. The experimental set-up and its output characteristics are discussed. Also, the applications of fiber OPAs are discussed and the one that we have exploited for our research.

In Chapter 3, we discuss the application of fiber OPA in WDM amplification and need for its gain control. Then we introduce the all-optical gain

clamping (AOGC). Then the experimental set-up for gain-clamping in a fiber OPA is shown, and its results are shown and discussed.

In Chapter 4, we introduce the fiber OPO. Then we divide it into Sections 4.1 and 4.2. In 4.1 we have shown the work on a watt-level output power and ultrawide tuning range CW fiber OPO centred at 1561 nm. Its output characteristics in terms of linewidth are also discussed. In section 4.2 we have discussed the work done on a CW fiber OPO centred at 1593 nm, with record tuning range and high output power. Saturation effects and pump power adjustment are also discussed.

In Chapter 5, we introduce fiber Raman amplification. A novel hybrid structure (fiber OPO to provide large seed, followed by fiber Raman amplification) designed to yield multi-watt output power, is introduced. The results are then presented and discussed.

In Chapter 6, we introduce stimulated Brillouin scattering and ways of suppressing it. Then multi-tone RF phase modulation is introduced and its impact on SBS is investigated. It is then compared to PRBS phase modulation in terms of SBS threshold increase, and price.

In Chapter 7 we discuss the work done on this research, and future possibilities.

References

1.1 P. A. Franken, A. E. Hill, *C.* W. Peters, and G. Weinreich, "Generation of optical harmonics," *Phys. Rev. Lett.,* vol. 7, p. 118, 1961.

1.2 C. C. Wang and *G.* W. Racette, "Measurement of parametric gain accompanying optical difference frequency generation," *Appl. Phys. Lett.*, vol. 6, p. 169, 1965.

1.3 R. H. Kingston, "Parametric amplification and oscillation at optical frequencies,"Proc. *IRE,* vol. 50, p. 472, 1962.

1.4 N. M. Kroll, "Parametric amplification in spatially extended media and the application to the design of tunable oscillators at optical frequencies," Phys. *Rev.,* vol. 127, p. 1207, 1962.

1.5 M. E. Marhic, N. Kagi, T.-K. Chiang, and L. G. Kazovsky, "Broadband fiber optical parametric amplifiers," *Opt. Lett.* vol. 21, p. 573, 1996

1.6 Min-Chen Ho Uesaka, K. Marhic, M. Akasaka, Y. Kazovsky, L.G., "200-nm Bandwidth Fiber Optical Amplifier Combining Parametric and Raman Gain," *J. Light-wave Technol.*, vol. 19, p. 977, 2001.

1.7 F. Forghieri, R. W. Tkach, A. R. Chraplyvy, and D. Marcuse, "Reduction of Four-Wave Mixing Crosstalk in WDM Systems Using Unequally Spaced Channels," *IEEE Photon. Technol. Lett.,* vol.6, p. 754, 1994.

1.8 B. P. P. Kuo, P. C. Chui, and K. K. Y. Wong, "A comprehensive study on cross-talk suppression techniques in fiber optical parametric amplifier by modulation format," *IEEE J. Select. Topics Quantum Electron.*, vol. 14, p. 659, 2008.

1.9 R. G. Smith, "Optical power handling capacity of low loss optical fibers as determined by stimulated Raman and Brillouin scattering", *Appl. Opt.* vol. 11, p. 2489, 1972

1.10 D. Cotter, "Observation of stimulated Brillouin scattering in low-loss silica fiber at 1.3 μm", *Electron. Lett.* vol. 18, p. 495, 1982

1.11 Yasuhiro Aoki, Kazuhito Tajma, and Ikuo Mito, "Input Power Limits of Single- Mode Optical Fibers due to Stimulated Brillouin Scattering in Optical Communication Systems", *J Light-wave Technol.*, vol. 6, p. 710, 1988.

1.12 S. K. Korotky, P. B. Hansen, L. Eskildsen, and J. J. Veselka, "Efficient Phase Modulation Scheme for Suppressing Stimulated Brillouin Scattering," in *Tech. Dig. Int. Conf. Integrated Optics and Optical Fiber Comm.*, vol. 1, paper WD2–1, p. 110, Hong Kong, 1995.

1.13 J.D. Marconi, J.M. Chavez Boggio and H.L. Fragnito, "Narrow linewidth fiber-optical wavelength converter with strain suppression of SBS", *Electron. Lett.*, vol. 40, 2004.

1.14 J. Hansryd, F. Dross, M. Westlund, P. A. Andrekson, and S. N. Knudsen, "Increase of the SBS Threshold in a Short Highly Nonlinear Fiber by Applying a Temperature Distribution", *J Lightwave Technol.*, vol. 19, p. 1691, 2001.

Chapter 2

Fiber Optical Parametric Amplification

2.1 Introduction

Optical parametric amplification (OPA) in fibers is based on the four-wave mixing (FWM) process [2.1] [2.2][2.3]. Availability of new high output power light sources, and commercialization of optical fibers with nonlinearity coefficient almost 10 times higher than for conventional fibers [2.4], has increased the interest in fiber optical parametric amplifiers. Unlike other types of optical amplifiers, they can provide amplification over large bandwidths. For instance, Erbium-doped fiber amplifiers (EDFAs) have gain bandwidth of only about 30 nm, while fiber OPAs can give amplification over hundreds of nanometres[2.5][2.6].

In Section 2.2 of this chapter, the FWM basis of one pump fiber OPAs is described. Also the gain equations and their parameters are discussed. In Section 2.3, the experimental setup for a fiber OPA that we investigated is given, and experimental results are discussed. Section 2.4 depicts the OPA gain spectra dependence on pump wavelength. Section 2.5 consists of a brief description of applications of fiber OPAs, and the applications that we investigated in our lab.

2.2. Four wave mixing and gain equations for one-pump fiber OPA

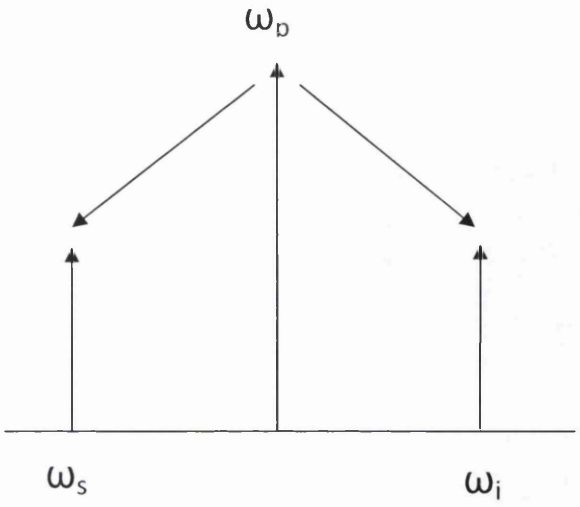

Fig.2.1 Frequency assignments for FWM in fibers.

For the single pump fiber OPA, we need to consider the degenerate-pump case. If ω_p is the pump frequency, ω_s is the seed signal frequency, and ω_i is the corresponding conjugate idler frequency, then we can write the equation between frequencies as [2.1]

$$2\omega_p = \omega_s + \omega_i \qquad [2.1]$$

The linear phase matching requirement for FWM is

$$\Delta\beta = 0; \text{ where } \Delta\beta = \beta_s + \beta_i - 2\beta_p \quad , \qquad [2.2]$$

where β is the propagation constant, which is a function of frequency.

Taking the nonlinear phase shift into account, the total phase mismatch term becomes

$$\kappa = \Delta\beta + 2\gamma P_0 \qquad [2.3]$$

where, γ is the nonlinearity coefficient of the fiber, given by the expression $\gamma = \frac{2\pi n_2}{\lambda_p A_{eff}}$, where n_2 is the nonlinear refractive index due to a high-intensity wave propagating in the medium, λ_p is the pump wavelength, A_{eff} is the effective core area of the fiber, and P_0 is the incident pump power.

The small-signal parametric gain expression can be found as in [2.1]

$$Gs(L) = \frac{|Es(L)|^2}{|Es(0)|^2} = 1 + \left[\frac{\gamma P_0}{g}\sinh(gL)\right]^2 \qquad [2.4]$$

where, $g = \sqrt{(\gamma P)^2 - (\kappa/2)^2}$, [2.5]

and L is the fiber length.

Using a Taylor expansion around the pump frequency, Eq. [2.2] can be written as:

$$\Delta\beta = 2\sum_{m=1}^{\infty} \frac{\beta_{2m}}{2m!}(\omega_s - \omega_p)^{2m} \qquad [2.6]$$

where β_{2m} denotes the $2m^{th}$ derivative of β at the pump angular frequency (ω_p)

It is clear that by tailoring the fiber dispersion properties, and choosing the right pump wavelength, fiber OPA gain bandwidth and spectrum shape can be altered. Also, by looking at Eq. [2.4], it is clear that $\Delta\beta$ is a function of only even powers of (ω_s-ω_p), and by combining Eq. [2.4] with Eq. [2.3], we see that the gain spectrum is independent of the odd orders of the dispersion; only even orders of dispersion contribute in the gain spectrum of fiber OPAs.

Considering the perfect phase matching conditions (κ = 0), the gain for the fiber OPA can be written as:

$$G = 1 + \exp(2\gamma PL)/4 \qquad [2.7]$$

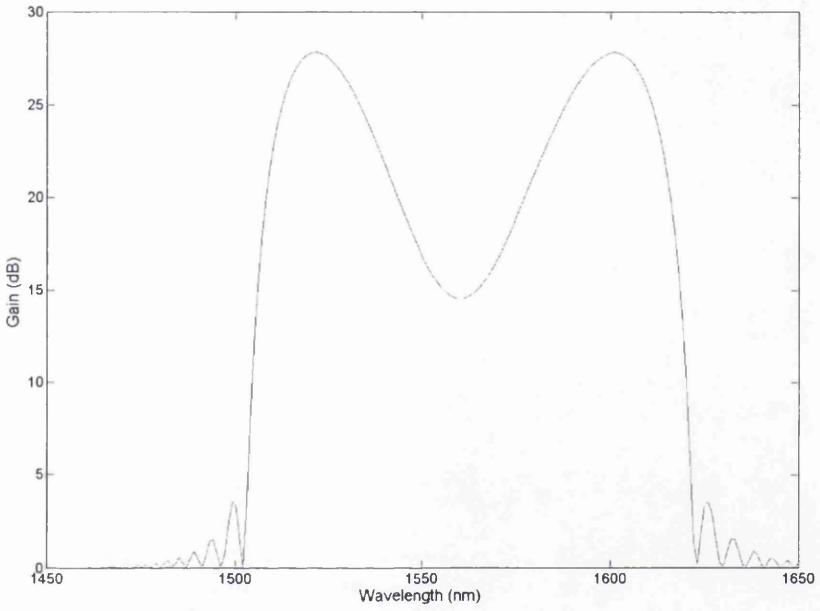

Fig. 2.2 Simulated OPA spectra

Figure 2.2 depicts a simulated fiber OPA gain spectrum. The parameters considered for simulations were as follows: fiber length of 350 m: input pump power of 1 W: fiber ZDW 1560 nm: pump wavelength (λ_p) 1561 nm; nonlinearity coefficient of fiber 15 $W^{-1}km^{-1}$.

2.3 Experimental set-up for fiber OPA, and gain spectra

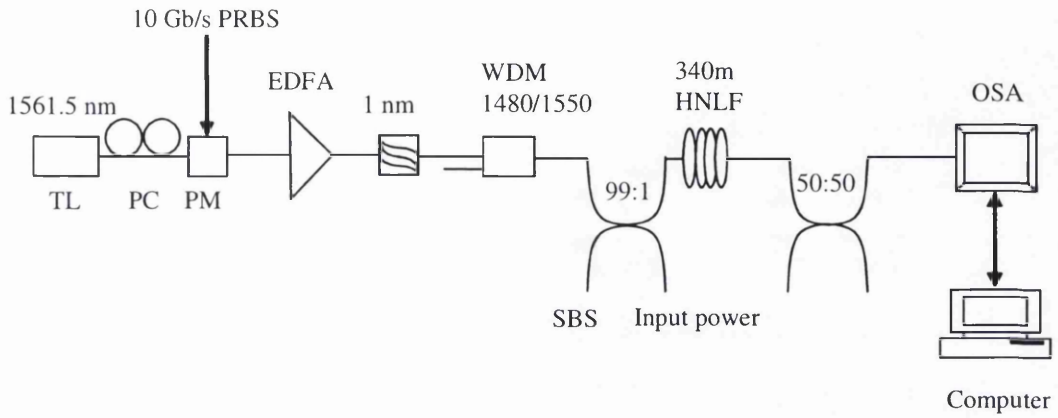

Fig. 2.3 Experimental set-up for the fiber optical parametric amplifier.

Figure 2.3 depicts the experimental set-up for the fiber OPA. A tunable laser (TL) serves as the pump at wavelength (1561.5 nm). It passes through a polarization controller (PC) to align the state of polarization with the phase modulator (PM). PM is driven by a 10 Gb/s pseudo-random bits sequence (PRBS) to suppress the stimulated Brillouin scattering (SBS). Then it passes through a 3-W Erbium-doped fiber amplifier to boost the pump. It then passes through the 1-nm bandwidth tunable bandpass filter (TBPF), to suppress the amplified spontaneous emission (ASE). It is then followed by a 1480/1550 nm wavelength division multiplexer (WDM), which has very low insertion loss at the pump wavelength (less than 1 dB); the other port (1480 nm) is used to launch the signal into the system. A 20-dB coupler was used for the purpose of keeping track of input powers and back reflected light. Then the pump passes through an HNLF, which has a length of 340 m. The nonlinearity coefficient

is about 15 $W^{-1}km^{-1}$, and the ZDW is 1560 nm. Then the output passes to the OSA, after attenuation.

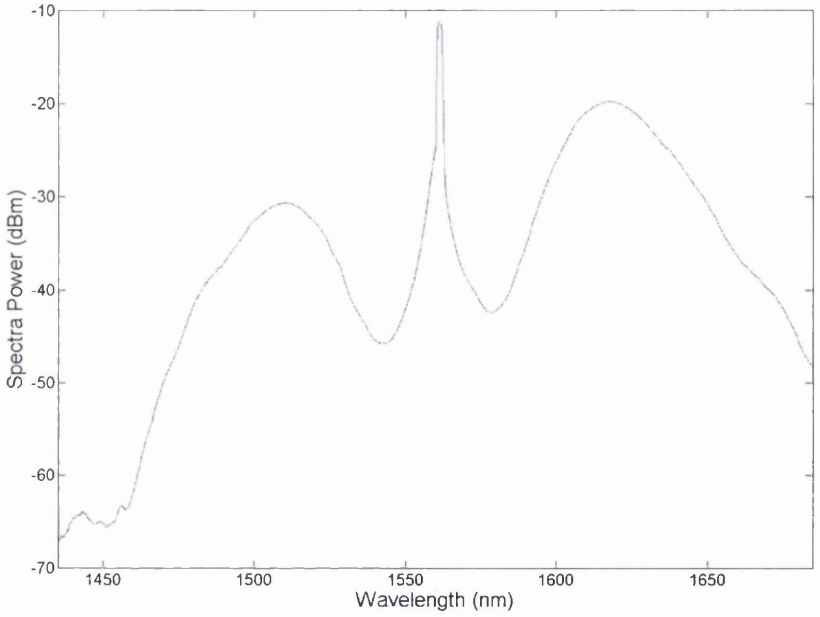

Fig.2.4 Experimental fiber OPA spectrum observed with 1561.5 nm pump wavelength.

Figure 2.4 shows the fiber OPA spectrum obtained experimentally using 2 W of input pump power. It shows a gain-bandwidth in excess of 200 nm. The idler asymmetry is due to the Raman gain contribution. The Raman gain contribution is from both the real and imaginary parts of the third-order susceptibility; it is less pronounced at lower pump power. More on the Raman contribution to the parametric gain will be discussed in Chapter 3.

2.4 Fiber OPA bandwidth vs pump wavelength

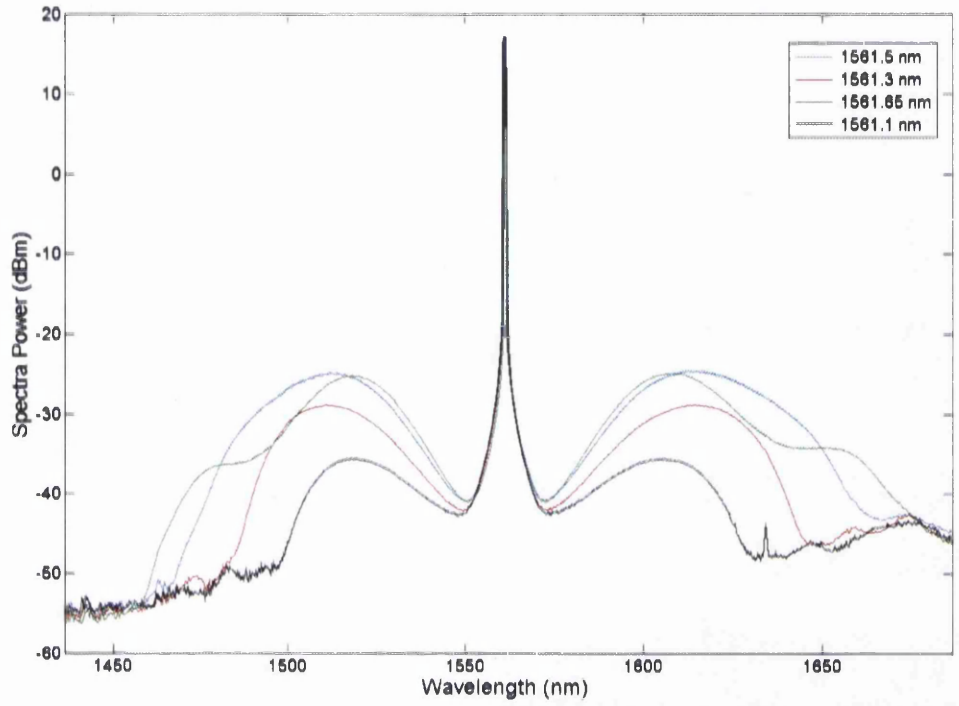

Fig. 2.5 Fiber OPA output spectra corresponding to different pump wavelengths

Figure 2.5 shows the experimental fiber OPA output spectra for 30 dBm of pump power, for different pump wavelengths around the ZDW. Slight changes lead to prominent changes in the shape and bandwidth of the fiber OPA spectra. Corresponding to the pump wavelength of 1561.5 nm, the bandwidth and the gain are optimum. This spectrum is shown in blue.

2.5 Applications of fiber OPAs

The most sought after attribute of any amplifier is its bandwidth. Broad-bandwidth fiber OPAs have been reported. In reference [2.5], dispersion shifted fiber (DSF) was used as the nonlinear medium, and gain was measured over a bandwidth of 35 nm. With HNLF coming into the market, with their nonlinearity coefficient (γ) as high as 25 $W^{-1}km^{-1}$, bandwidths of fiber OPAs have been reported in the hundreds of nanometers [2.6]. The HNLFs, generally speaking, have low dispersion in comparison to DSF. Choosing the pump wavelength near the ZDW of the fiber, fiber OPA bandwidth can be optimized. Slight changes of wavelength can give different gain shapes, and a suitable wavelength can be chosen to optimize both gain and bandwidth.

Since ultra-wide bandwidth fiber OPAs have been reported, they also had applications as potential supercontinuum sources. This will be discussed in brief in the Chapter 3.

A CW fiber OPA with a signal gain of 70 dB has been reported by Torounidis et al. [2.7]. They used 2 W of CW pump power, and 500 m of HNLF. This gain is larger than could be achieved from other type of amplifier, such as EDFAs and Raman amplifiers.

Fiber OPAs can find applications in phase conjugation as well, since the idler's phase is opposite to the phase of the signal. This application can be used against some nonlinear effects, such as cross phase modulation, or against dispersion.

Since fiber nonlinearity response is almost instantaneous, modulation of the pump will be transferred to both the signal and the idler. This feature can be used in regeneration of signals, and demultiplexing high-speed TDM signals.

A fiber OPA with a noise figure of 3.7 dB was reported by Voss, P.L. et al. [2.8]. This noise figure is as good as achieved with other amplifiers such as EDFAs and Raman amplifiers. Recently a lot of work has been done on phase-sensitive fiber OPAs (PSAs). Noise figure of 1.1 dB has been reported in PSAs by the Chalmers group [2.9].

Fiber OPAs may also find applications in photonic networks, as they provide such a large bandwidth to multiplex wavelengths that are far from each other. But with this application are associated some detrimental nonlinear effects, such as FWM and cross gain-modulation (XGM). Different modulation techniques have been tried to minimize the cross gain modulation (XGM) effects [2.10]. Also, it has been reported that FWM can be reduced if unequal spacings are used between channels [2.11]. All-optical gain clamping (OGC) has also been reported, but only theoretically [2.12]. In the second chapter we shall present the experimental work that we did on gain-clamping in fiber OPAs, for their application in photonic networks.

Putting such a broadband and high-gain medium between two mirrors, oscillation can be obtained at any wavelength from the S-band to the U-band. This is known as a fiber optical parametric oscillator (fiber OPO). This gives us a very powerful light source. This application is the main theme for Chapter 4.

Since fiber OPAs provide such large bandwidth, wavelength conversion can be achieved at wavelengths where light sources are very rare. So fiber OPAs, or fiber

OPOs, can be used to seed Raman amplification to generate very high ouput powers at those wavelengths. This is the main theme for Chapter 5.

The pump requirements for making such broadband and high-gain fiber OPA is of the order of a few watts, when DSF or HNLF is used. For such power levels, stimulated Brillouin scattering (SBS) can pose a significant problem. It puts a constraint on how much power we can launch into the fiber. There are several available techniques to suppress SBS, for instance putting strain into the fiber, phase or frequency dithering of the pump, etc. Although dithering the pump is the most common technique used, SBS suppression using multi-tone RF phase modulation is the main theme for Chapter 6.

References:

2.1 G. P. Agrawal, "Nonlinear Fiber Optics", fourth edition, Academic Press, San Diego, USA, 2007.

2.2 M. E. Marhic, "Fiber Optical Parametric Amplifiers, Oscillators and Related Devices", Cambridge, 2008.

2.3 R. H. Stolen and J. Bjorkholm, "Parametric amplification and frequency conversion in optical fibers", *IEEE J. Select. Topics Quantum Electron.*, vol. 18, p. 1062, 1982.

2.4 M. Onishi, T. Okuno, T. Kashiwada, S. Ishikawa, N. Akasaka and M. Nishimura, "Highly nonlinear dispersion-shifted fibers and their application to broadband wavelength converter", *Opt. Fiber Technol.*, vol. 4, p. 204, 1988.

2.5 M. E. Marhic, N. Kagi, T.-K. Chiang, and L. G. Kazovsky, "Broadband fiber optical parametric amplifiers," *Opt. Lett.* vol. 21, p. 573, 1996.

2.6 K. Min-Chen Ho Uesaka, M. Marhic, Y. Akasaka, L.G. Kazovsky, "200-nm Bandwidth Fiber Optical Amplifier Combining Parametric and Raman Gain," *J. Light-wave Technol.*, vol. 19, p. 977, 2001.

2.7 Torounidis T., Andrekson, P. A., and Olsson, B.E, "Fiber Optical Amplifier With 70-dB Gain," *IEEE Photon. Technol. Lett.*, vol. 18, p. 1194, 2006.

2.8 P. L. Voss, R. Y. Tang and P. Kumar, "Experimental measurement of the photon statistics and noise figure of a parametric fiber amplifier", *Optics Letters*, vol. 28, p. 549, 2003.

2.9 R. Slavik, F. Parmigiani, J. Kakande, C. Lundstrom, M. Sjodin, P. A. Andrekson, R. Weerasuriya, S. Sygletos, A. D. Ellis, L. Gruner-Nielsen, D. Jakobsen, S. Herstrom, R. Phelan, J. O'Gorman, A. Bogris, D. Syvridis, S. Dasgupta, P. Petropoulos and D. J. Richardson, *Nature Photonics,* vol. 5, 2010.

2.10 B. P. P. Kuo, P. C. Chui, and K. K. Y. Wong, "A comprehensive study on cross-talk suppression techniques in fiber optical parametric amplifier by modulation format," *IEEE J Select. Topics Quantum Electron.*, vol. 14, p. 659, 2008.

2.11 F. Forghieri, R. W. Tkach, A. R. Chraplyvy, and D. Marcuse, "Reduction of Four-Wave Mixing Crosstalk in WDM Systems Using Unequally Spaced Channels," *IEEE Photon. Technol. Lett.,* vol.6, p. 754, 1994.

2.12 N. Gryspolakis, and L. R. Chen, "Response of fibre optic parametric amplifiers to channel add/drop in agile all-photonic networks," *Optics Communications*, vol. 278, p. 168, 2007.

Chapter 3

All-optical gain clamping in fiber optical parametric amplifiers

3.1 Introduction

WDM amplification using fiber OPA has been previously studied. The point of attention has been optimizing the fiber OPA parameters, such as the dispersion properties of the fiber, using two pumps to get a flattened gain spectrum, etc. This kind of amplifier works well for specific operating conditions, like fixed number of channels, with specific input power of the signals [3.1][3.2][3.3]. Under these fixed conditions, methods have been proposed to mitigate the nonlinear effects such as XGM, and FWM [3.4] [3.5]. In reference 3.4 Kuo et al. showed that RZ DPSK modulation can reduce the FWM and XGM to a good extent. In reference 3.5 it has been reported that if the channel spacing is kept uneven, FWM problems are reduced.

However, in modern WDM network systems, the operating conditions are not fixed. It becomes clear that as parameters such as number of input signals, and signal input power change, the performance of a fiber OPA will be degraded. Therefore, any conclusions drawn from the research on multi-channel fiber OPA cannot entirely be applied to reconfigurable network systems. In order to consider fiber OPAs as a potential candidate for agile, WDM photonic networks, their performance has to be evaluated under varying operating conditions.

In agile WDM photonic networks the number of channels passing through an amplifier changes according to the demand for bandwidth, because of network reconfiguration, and component failures that result in one or more channels being

dropped. Even if the number of channels can be kept constant, channel input power changes, on the basis of packet level, and on the basis of different optical distances travelled. Consequently total signal input power to an amplifier varies with time. So, we have studied the behaviour of a fiber OPA under such circumstances, by considering the effects of change of total input power, and add/drop of channels on the gain characteristics.

Also, study of the behaviour of fiber OPAs in active photonic networks carrying data becomes very important. For this application, fiber OPAs should have low output power transients. Broadly speaking, amplifiers operate near saturation, in order to have optimized efficiency, and best noise performance. In this case, the total output power of a saturated amplifier is nearly constant, independent of the number of channels involved. But the gain experienced by each channel will depend on the number of channels present. These transients due to adding and dropping of channels have been studied both theoretically and experimentally in other optical amplifier, including EDFAs [3.6][3.7][3.8][3.9], RAs [3.10][3.11][3.12], Thulium-doped fiber amplifiers [3.13][3.14], and semiconductor optical amplifiers [3.15]. In fiber OPAs, no experimental work has been done so far in this regard: only a theoretical investigation has been performed [3.16].

This part of the thesis is towards the study the fiber OPAs for their applications in photonic networks. Section 3.2 of the chapter describes the techniques that have been used to tackle the problems mentioned above in optical amplifiers. Section 3.3 describes the technique we chose for fiber OPAs. Section 3.4 illustrates the experimental set-ups and results for saturation effects in fiber OPA. Section 3.5 discusses the experimental set-up and results for the add/drop response of the fiber OPA. Section 3.6 contains the cross gain modulation results. Section 3.7

states the BER measurements. Section 3.8 states the FWM effects on this particular case. And in Section 3.9 we conclude the chapter.

3.2 Gain-control techniques

As discussed earlier, for using fiber OPAs in dynamic photonic networks, their gain needs to be controlled. Gain control technique has been studied in depth for other type of amplifiers, including EDFA, TDFA, and RAs. Here we give a brief introduction of these techniques.

3.2.1 Using pump control techniques

Gain control of an amplifier by controlling its pump was one the first techniques to be employed, by M Karasek et al [3.17]. They used this technique to control the gain of Raman amplifiers. In this technique, a small portion of the output is tapped, while the monitor channel that was fed into the amplifier is filtered out and used to define an electrical signal to the pump diode. Changes in signal input power give changes in the defined electrical signal, which in turn modifies the pump power. This way the gain remains constant. But this technique comes with a lot of complexity, such as electronic circuits, and the almost instantaneous response time required poses some problems. Moreover, this technique will even be harder to use with fiber OPAs, because of FWM generation.

3.3 All-optical gain clamping (AOGC)

This technique was first utilised in other types of amplifiers, e.g. EDFAs, Raman amplifiers (RA), and Thulium-doped fiber amplifiers (TDFA). It can be classified

into two categories: standing-wave AOGC with fiber Bragg gratings (FBGs) as mirrors to select the lasing signal; travelling-wave AOGC using ring resonator with the help of fiber couplers. Gain-clamping based on ring resonators has some added advantages over the standing-wave AOGC: one is that by using a tunable bandpass filter (TBPF) the lasing signal wavelength can be changed, and by using a variable optical attenuator (VOA), different levels of gain clamping can be achieved. For these reasons we have used travelling-wave AOGC using a ring resonator in our fiber OPA.

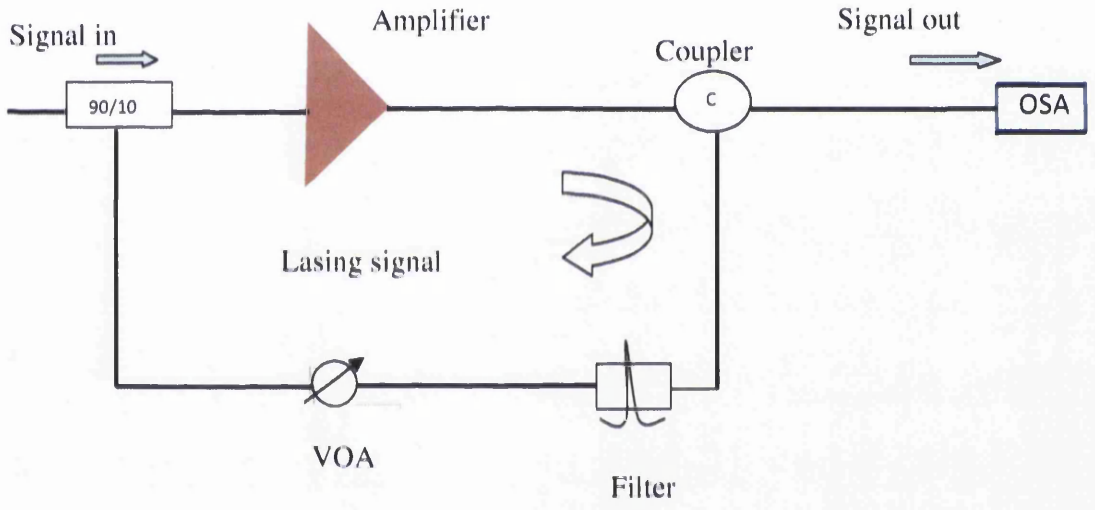

Fig. 3.1 Typical set-up for OGC for an amplifier

Figure 3.1 shows the typical experimental set-up for gain clamping in fiber amplifiers. The loop is formed using fiber couplers, a TBPF, and a VOA . The lasing signal wavelength is always selected to be different than that of the amplified signal. Any change in the gain is compensated by the lasing wave amplitude, and the gain for amplifying the signal ideally stays the same. With this technique, the gain of the

signal is clamped to a value equal to the losses of the cavity, and any increase in the pump power wouldn't increase the gain. This technique can be very helpful, when these amplifiers are used for applications in photonic networks, where numbers of channels may be added/dropped, which leads to gain variations for the other channels.

3.4 Gain clamping set-up for the fiber OPA

3.4.1. Experimental set-up

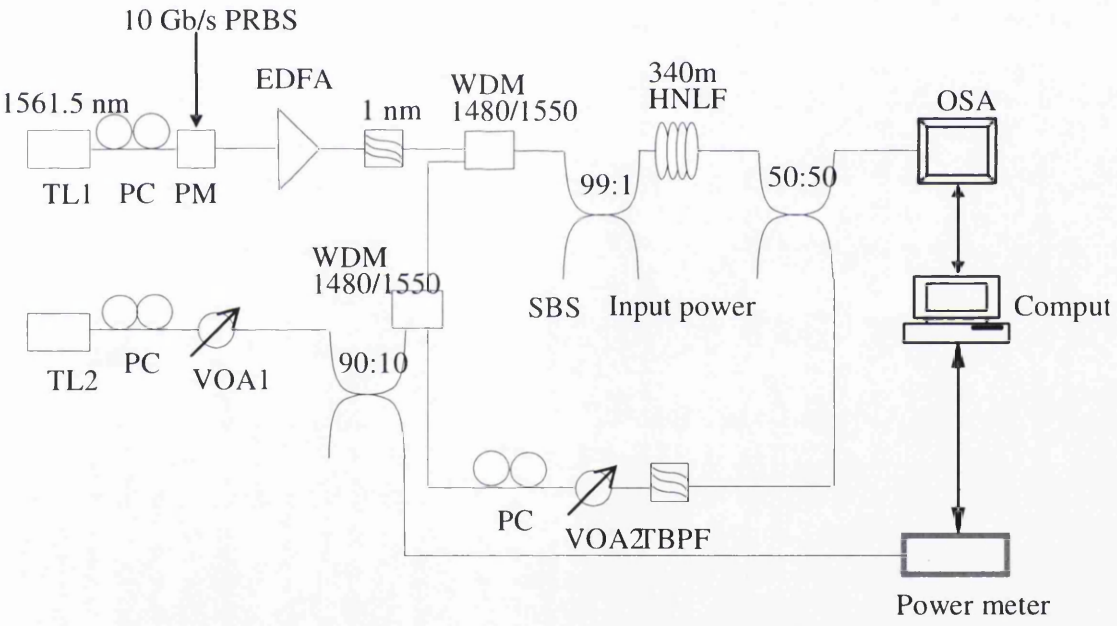

Fig. 3.2 Experimental set-up for gain clamping in fiber OPAs.

Figure 3.2 shows the experimental set-up for gain clamping in fiber OPAs. Tunable laser (TL1), with a wavelength of 1561.5 nm, was used as the OPA pump source. It passed through a PC to align the axis of the next PM with the pump. The

PM was driven by a 10 Gb/s PRBS. Pump was phase dithered in order to avoid SBS. The pump was then amplified by high-output-power amplifiers (EDFAs), to a level of up to 3 W. The ASE from the EDFA was filtered out by a band-pass filter centred at the pump wavelength. The signal was taken from another tunable laser (TL2), which passed through a polarization controller to maximize the OPA gain, and then through a VOA1, to vary the signal input power. The pump and the signal were then combined by a broadband WDM (1480/1550 nm), and injected into a 340-m long HNLF through a 20-dB coupler. One power meter was placed after the coupler to monitor the power injected into the fiber, and another one measured the pump power reflected by SBS. The output from the HNLF then passed through a 3-dB coupler, which coupled half of the power into the feedback loop; the other attenuated half went to the OSA, which was controlled by a computer through GPIB. In the loop we had a TBPF, which determined the lasing wavelength (1535 nm), which was different from the signal wavelength (1520 nm). After TBPF, VOA2 was used to set different levels of gain-clamping. Then we used a PC, to maximize the lasing signal power. A second WDM coupler was used to launch the signal into the HNLF. Another power meter was used to keep track of the signal input power to the HNLF; it was controlled by the same computer as the OSA.

3.4.2 Results

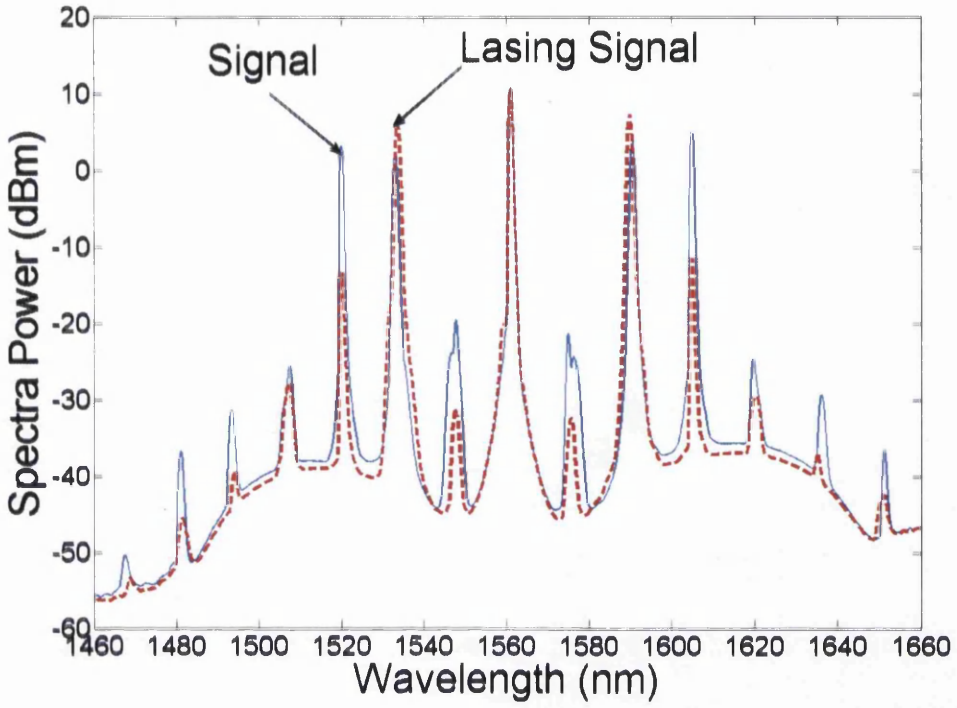

Fig. 3.3 Gain-clamped fiber OPA spectra with signal on. Lasing signal is at 1530 nm, and the seed signal is at 1520 nm.

Figure 3.3 shows the basic working principle of the gain-clamped fiber OPA. The approach that we chose for implementing OGC is that of controllable lasing in the bandwidth of the amplifying medium (OPA). The basic principle is to establish, by means of fiber couplers, a feedback path containing a tunable narrowband filter and a VOA. By controlling these components, it is possible to obtain laser oscillation at an arbitrary wavelength, with an adjustable intensity. For high lasing levels, the pump power is depleted, and the gain for the other signal wavelengths is reduced. Under these conditions, the gain variations caused by the changes in the signal input power are greatly reduced, compared to what happens under the open-loop conditions.

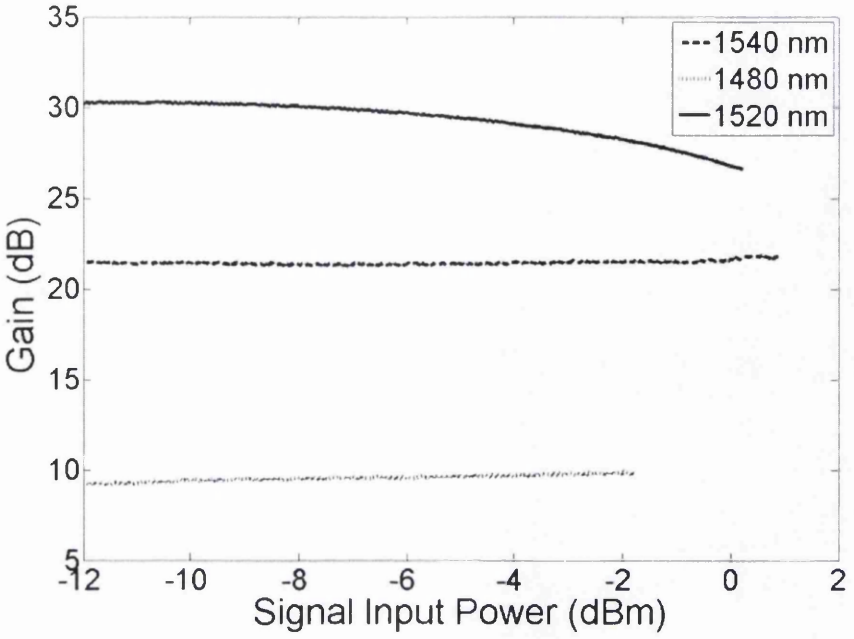

Fig. 3.4 Open loop fiber OPA gain versus signal input power

Figure 3.4 shows the variation of the open loop (gain-clamping off) fiber OPA gain versus signal input. It was observed at three wavelengths: 1520 nm (centre and peak of the gain spectra), and at 1480 and 1540 nm (at the edges of the gain spectra). At 1520 nm, where the gain is maximum, gain variation is slightly over 4 dB, with signal input power variation from -12 dBm to 0 dBm. By contrast at 1480 and 1540 nm, the gain doesn't vary much with signal input power variation. This is for the simple reason that gain close to the pump and far away from it are lower, so we don't see any gain saturation. But at the peak of the gain, the signal sees saturation. As we discussed earlier, when an amplifier is operated in saturation, the gain for a signal depends on the number of channels present. So, adding or dropping

of channels will reduce or increase the gain for the surviving signals. Therefore, saturation has to be avoided for fiber OPAs to use in WDM photonic networks.

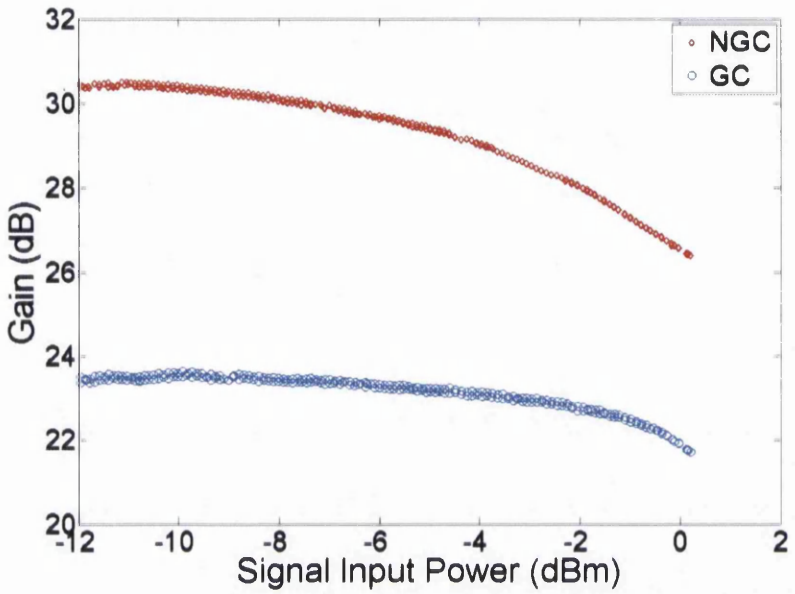

Fig. 3.5 Fiber OPA gain variation with signal input variation, red lozenges depicts no gain clamping case, while blue circle depicts the clamping on case.

Figure 3.5 shows the fiber OPA gain variation under gain-clamping off (solid red line), and gain-clamping on (dotted blue line) versus signal input power variation from -12 dBm to 0 dBm. The signal wavelength was kept at 1520 nm, while the lasing signal wavelength was 1540 nm. When there is no gain clamping, shown by red cubes, the gain varies up to 4 dB, with an input signal power variation of more than 12 dB. While, when the gain-clamping is on, the gain variation is only 1 dB with signal input power variation from -12 dBm to 0 dBm. The saturation ceases to exist because the lasing signal depletes the pump, which reduces the gain.

3.4.3 Gain-flattening

One-pump fiber OPA gain spectra are not very flat. The gain varies quite a bit with wavelength (See Fig. 3.6). For applications in photonic networks, it would be good for the gain spectrum to be almost flat, so all the channels (at different wavelengths) would see similar gains.

.

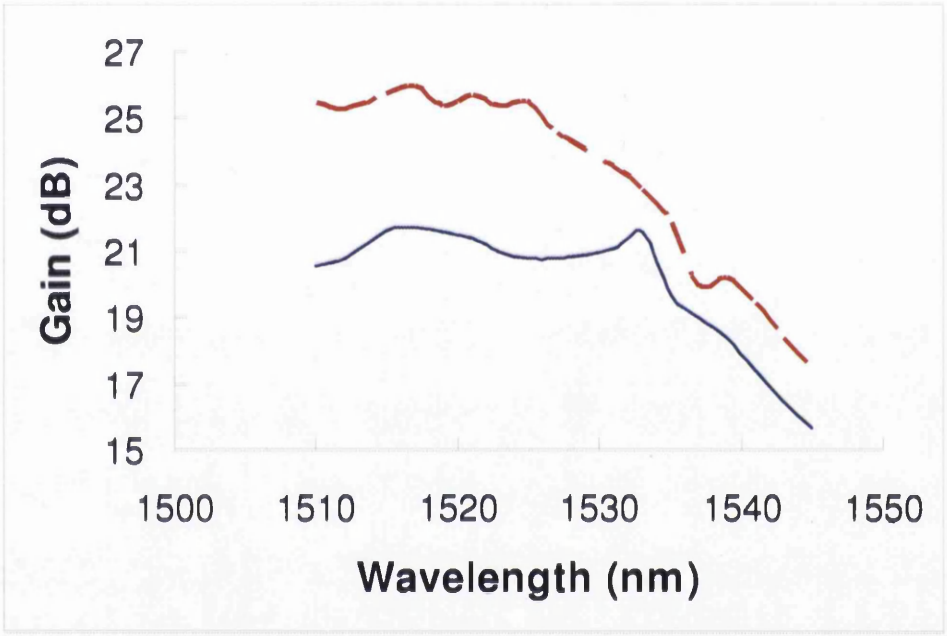

Fig. 3.6 Fiber OPA gain variation vs signal wavelength, under gain clamping (blue continuous line), and without gain clamping (red dotted line)

Figure 3.6 shows the fiber OPA gain variation versus signal wavelength. Red color depicts when the gain clamping is off, and blue color depicts when the gain clamping is on. Without gain clamping the gain variation is more than 8 dB, while this is reduced to 4 dB when the gain clamping is on.

3.5 Channels add/drop response of fiber OPA

This section covers the response of fiber OPA against the adding dropping of channels. How it affects the gain of the surviving channels, how it affects the data sent through the signals, and how it affects the bit error rate (BER) of the system. From experimental data we show that AOGC mitigates these problems, and makes the system better for its application in WDM photonic networks.

3.5.1 Experimental set-up

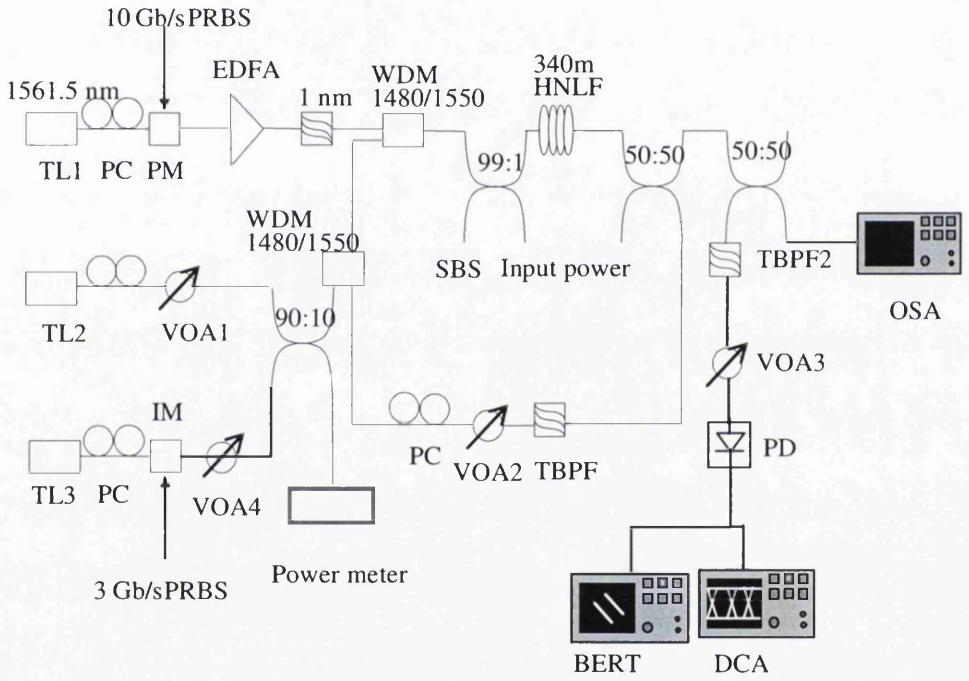

Fig. 3.7 Experimental set-up for observing the transients in fiber OPA.

The experimental setup is shown in Fig. 3.7. Tunable laser TL1, with a wavelength of 1561.5 nm, was used as the OPA pump source. Its output passed through a phase modulator (PM) for suppressing SBS. The PM was driven by a 10 Gb/s PRBS. The pump was then amplified by high-output-power EDFA, to a level of up to 3 W. The ASE from the EDFA was filtered out using a bandpass filter centred at the pump

wavelength. Tunable lasers TL2 and TL3 were respectively used to provide: (i) a controllable high-power wave to simulate adding/dropping a group of signals; (ii) a low-power input signal considered to test signal amplification, with and without the high-power wave. Both passed through a polarization controller (PC) to maximize the OPA gain, and then through a variable optical attenuator (VOA1), to vary the signal power. The second signal, provided by TL3, was intensity-modulated by a 3 GHz PRBS, to observe cross-gain modulation. These two signals were combined using a 90/10 coupler. The pump and the two signals were then combined by a broadband WDM, (1480 nm/1550 nm), and injected into a 340-m long HNLF through a 20-dB coupler. A power meter was placed after the coupler to monitor the power injected into the fiber, and another one measured the pump power reflected by SBS. The output from the HNLF then passed through a 3-dB coupler, which coupled half of the power into the feedback loop. In the loop we had a TBPF, which determined the lasing wavelength (1535 nm), which was different from the signal wavelength (1520 nm). After TBPF, VOA2 was used to set different levels of gain clamping. We then used a PC to maximize the lasing signal power. A second WDM coupler was used to launch the signal into the HNLF. Another power meter was used to keep track of the add/drop signal input power to the HNLF.

The output of the cavity went to another 3 dB coupler, which sent half of the power to the OSA, while the other half went to TBPF2 to select the intensity-modulated signal. We then placed VOA3 to attenuate the power received by the photodiode (PD), to measure BER plots with the BERT.

3.5.2 Results

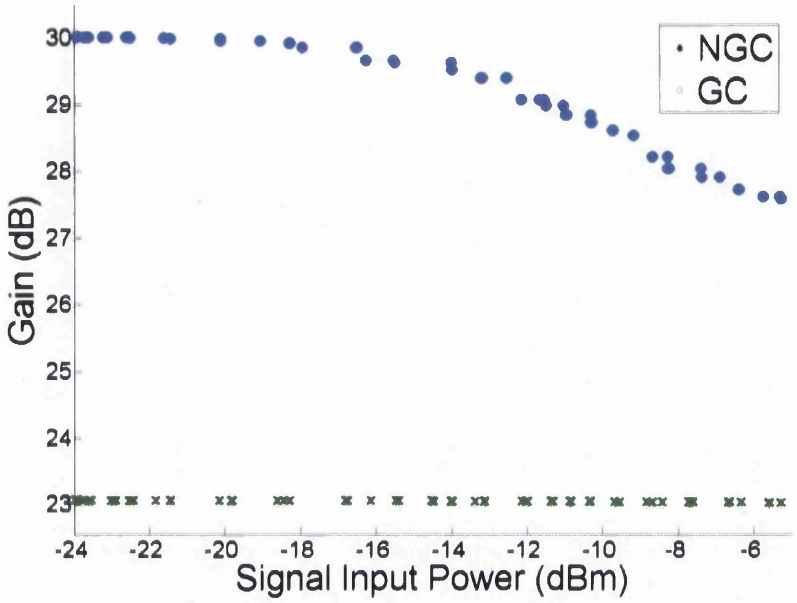

Fig. 3.8 Signal gain vs the other signal input power variations. Blue dots depict the no gain clamping case, green cross depicts the gain clamping on case.

Figure 3.8 shows the results depicting the effects of signal input power variations on other channels in WDM amplification systems. As we discussed earlier how the number of channels can be reduced or increased due to demand of bandwidth or components failure, this makes the signal input powers to the amplifier variable. The blue dots depict the gain of the signal, without gain clamping, when the other signal input power varies from -25 dBm to -5 dBm. The gain of the signal varies from 30 dB to 27 dB. The green crosses depict the gain of the signal, with gain clamping, under the same variation of power level of the other input signals. In this case, the gain variation is below 0.5 dB, as the gain is clamped by the lasing signal into the ring cavity. This is the ideal case for the WDM photonic networks,

and these results prove that AOGC in fiber OPA improves their capability of amplifying WDM signals.

3.6 Cross gain-modulation

Comparisons can be drawn from the results mentioned in the earlier section. Since gain clamping renders the signal gain of a fiber OPA immune from the other signal input power variations, cross gain modulation should also be zero. We can also call this curbing of transients using gain clamping. We prove this also by measurements. This was done by intensity-modulating a small signal using a 3 Gb/s PRBS. Its filtered output was observed on a DCA, when the other signals were manually added/dropped.

Figure 3.9 shows the effects of gain-clamping on cross gain modulation (XGM), when the large signal is added and dropped. In (a), the gain-clamping is off, and when the signal is added and dropped, the gain is strongly modulated, as a result of XGM. In this case the power fluctuations are of the order of 100 μW. By contrast in (b), when the gain-clamping is on, and the large signal is added/dropped, the power-fluctuations are almost non-existent.

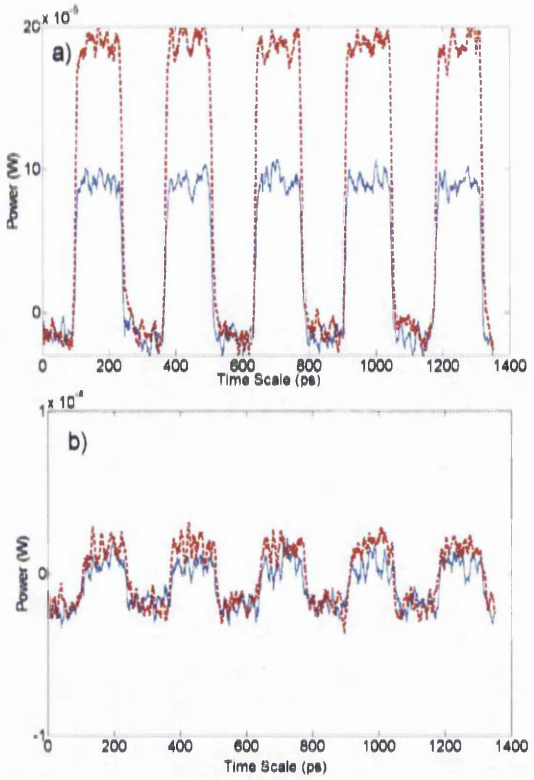

Fig. 3.9 Cross gain-modulation effects when the large signal is added/dropped (blue/red color); (a) when the gain-clamping is off; (b) when the gain-clamping is on.

3.7 Bit error rate (BER) measurements

Information is sent through optical fibers by modulation (phase and/or amplitude) of the signal. For digital transmission the information is sent as bits, i.e. 0 and 1. But due to noise, interference and distortion the number of bits received may be altered. The bit error rate (BER) is defined as the number of bit errors divided by the total number of bits transferred during a time interval.

In fiber OPAs the number of bits received is altered due to pump noise transfer to the signals, crosstalk between the channels, quantum noise, etc. In agile networks the adding and dropping of channels alleviates this problem.

As mentioned earlier, it was shown by Kuo et al. that RZ DPSK modulation not only reduces nonlinear crosstalk in a fiber OPA, but also improves the BER of the system. Power penalties were shown to be improved from 2.8 dB to 1.8 dB at the BER of 10^{-9}. But these results have been obtained with fixed parameters. They no longer hold when the number of input channels starts varying. This section studies the effect of adding/dropping of channels on the BER of the system, and how AOGC could improve it. The experimental setup stays the same as in Fig. 11, but now the BER of the intensity-modulated signal is measured as other signals are added and dropped.

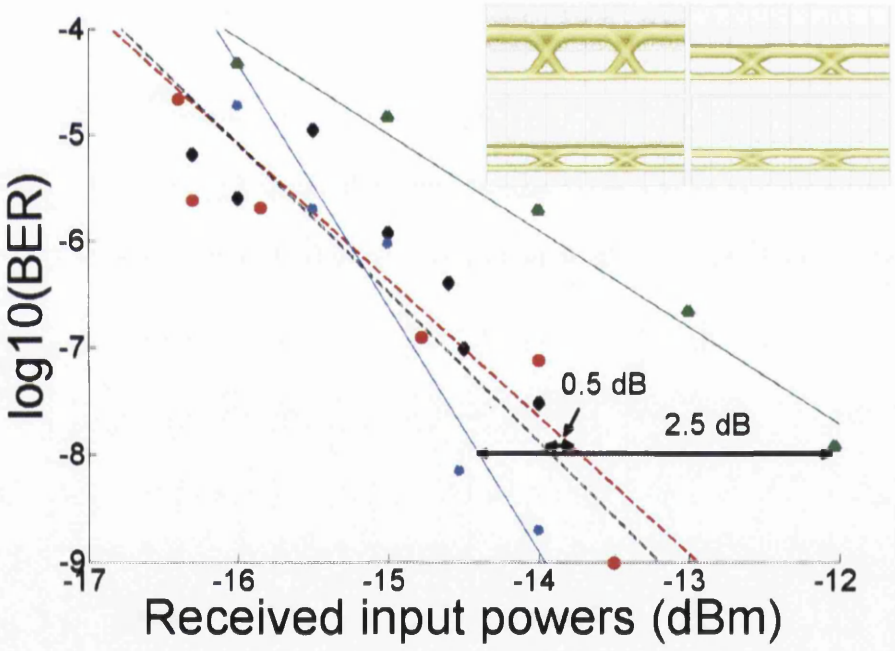

Fig. 3.10 Measured BER results of the system vs the input power received at the photo diode. Solid line depicts the no gain clamping case, while the dotted one shows the gain clamping on case.

Figure 3.10 displays the results obtained on the BERT. As can be seen from the figure, when there is no gain clamping (depicted by solid lines) the power penalties at the BER of 10^{-8} is about 2.5 dB, while with gain clamping on (depicted by dotted lines), the power penalties are improved from 2.5 dB to 0.5 dB. The conclusion can be drawn from these results that the signal quality is altered very little when different signals are added and dropped, under gain clamping of the fiber OPA.

3.8 Effects of four-wave mixing

One problem with fiber OPAs, when used in photonic networks, is FWM. If the signals are kept very close to each other, FWM becomes very prominent. Here we kept the lasing signal, add/drop signal, and intensity modulated signal reasonably far from each other to avoid FWM.

Figure 3.11 shows the gain-clamped OPA spectra, when the signal is dropped, while figure 3.12 shows the gain-clamped OPA spectra when the signal is added. In both cases, FWM peaks are very low in amplitude and do not contribute much.

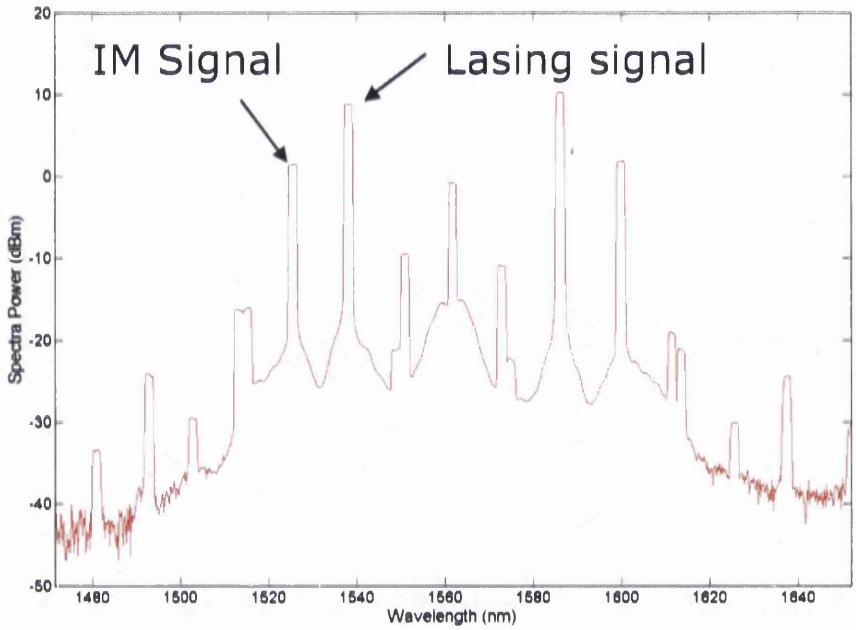

Fig. 3.11 Gain-clamped fiber OPA spectra when there is no add/drop signal

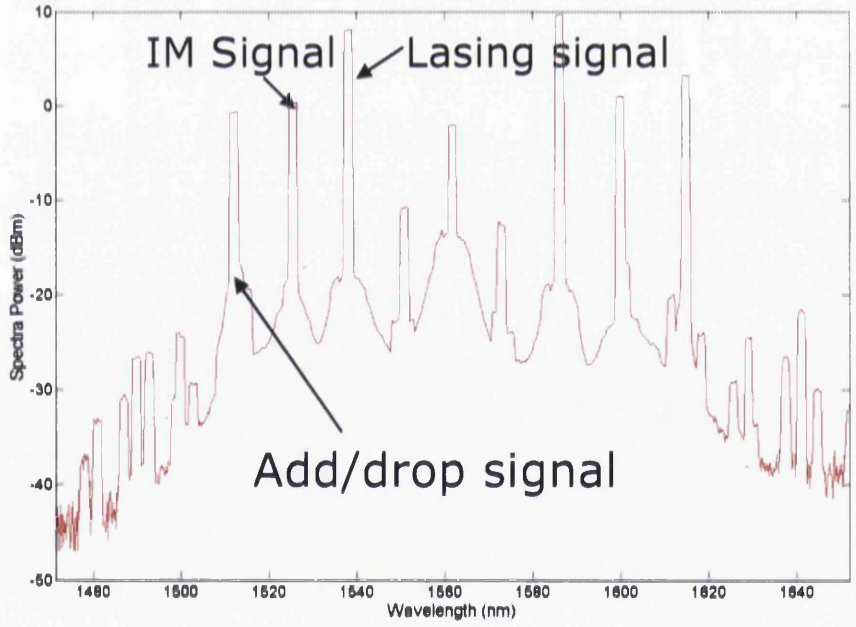

Fig. 3.12 Gain-clamped fiber OPA spectra when add/drop signal is on

Since we used one large signal for adding/dropping in order to simulate several channels, FWM doesn't affect our case. But it can be stated that AOGC doesn't mitigate the FWM, and other methods such as unequal channel spacing should be used in order to mitigate it.

3.9 Conclusion

We have reported an experimental investigation of all-optical gain clamping in fiber OPAs for their application in photonics networks, for the first time to our knowledge. We reduced signal gain variation down to 0.5 dB, for input signal power varying from -25 dBm to -5 dBm. Signal-gain saturation was also reduced by OGC. Cross-gain modulation when a high-power auxiliary signal was added or dropped was reduced to below 0.5 dB. Power penalties for a 3 Gb/s OOK signal were also improved from 2.5 dB to 0.5 dB at the BER of 10^{-8}. Signal-gain flatness was also improved by the presence of gain clamping. This work could help facilitate the introduction of fiber optical parametric amplifiers in optical communication networks.

References

3.1 C. J. McKinstrie, S. Radic and A. R. Chraplyvy, "Parametric amplifiers driven by two pump waves", *IEEE J. Select. Topics Quantum Electron.*, vol. 8, p. 538, 2002.

3.2 K. Y. Wong, M. E. Marhic, K. Uesaka and L. G. Kazovsky, "Polarization independent two-pump fiber optical parametric amplifier", *IEEE Photon. Technol. Lett.*, vol. 14, p. 911, 2002.

3.3 J. M. Chavez Boggio, J. D. Marconi and H. L. Fragnito, "Double-pumped fiber optical parametric amplifier with flat gain over 47-nm bandwidth using a conventional dispersion-shifted fiber", *IEEE Photon. Technol. Lett.*, vol. 17, p. 1842, 2005.

3.4 B. P. P. Kuo, P. C. Chui, and K. K. Y. Wong, "A comprehensive study on cross-talk suppression techniques in fiber optical parametric amplifier by modulation format," *IEEE J Select. Topics Quantum Electron.*, vol. 14, p. 659, 2008

3.5 F. Forghieri, R. W. Tkach, A. R. Chraplyvy, and D. Marcuse, "Reduction of Four-Wave Mixing Crosstalk in WDM Systems Using Unequally Spaced Channels," *IEEE Photon. Technol. Lett.,* vol.6, p. 754, 1994.

3.6 S. W. Harun, S. K. Low, P. Poopalan, and H. Ahmad, "Gain-clamping in L-band Erbium-doped fiber amplifier using a fiber Bragg grating," *IEEE Photon. Technol. Lett.*, vol. 14, p. 293, 2002.

3.7 S. H. Lee, and S. H. Kim, "All-optical gain-clamping in Erbium doped fiber amplifier using stimulated Brillouin scattering," *IEEE Photon. Technol. Lett.*, vol. 10, p. 1316, 1998.

3.8 L. Yi, L. Zhan, W. Hu, Q. Tang, and Y. Xia, "Tunable gain-clamped double-pass Erbium-doped fiber amplifier," *Opt. Express* vol. 14, p. 570, 2006

3.9 L. Yi, L. Zhan, C. Taung, S. Luo, W. Hu, Y. Su, Y. Xia, and Lufeng Leng, "Low noise figure all-optical gain-clamped parallel C+L band Erbium-doped fiber amplifier using an interleaver," *Opt. Express* vol. 13, p. 4519, 2005.

3.10 S. S.-H. Yam, M. E. Marhic, Y. Akasaka, and L.G. Kazovsky, "Gain-clamped S-band discrete Raman amplifier," *Opt. Lett.* vol. 29, p. 757, 2004

3.11 H. S. Seo, J. T. Ahn, B. J. Park, and W. J. Chung, "Gain-clamped Raman fiber oscillator," *Opt. Lett.* vol. 33, p. 327, 2008

3.12 Y. J. Rao, X. H. Jia, L. Li, and Z. L. Ran, "Detailed investigation on gain-clamping characteristics of ultralong fiber Raman laser using FBGs," *J. Opt. Soc. Am. B* vol. 26, p. 1334, 2009

3.13 S. Yam, F. An, M. Marhic, L. Kazovsky, "Gain-clamped Thulium-doped fiber amplifier with a single pump at 1050 nm," *OFC'03* paper FB3

3.14 S. Aozasa, H. Masuda, M. Shimizu, and M. Yamada, "Novel Gain Spectrum Control Method Employing Gain Clamping and Pump Power Adjustment in Thulium-Doped Fiber Amplifier," *J. Light-wave Technol.* vol. 26, p. 1274, 2008

3.15 X. H. Jia, "Theoretical investigation of gain-clamped semiconductor optical amplifiers using the amplified spontaneous emission compensating effect," *J. Opt. Soc. Am. B* vol. 23, p. 2503, 2006

3.16 N. Gryspolakis, and L. R. Chen, "Response of fibre optic parametric amplifiers to channel add/drop in agile all-photonic networks," *Opt. Commun.*, vol. 278, p. 168, 2007.

3.17 M. Karasek and M. Menif, "Protection of surviving channels in pumpcontrolled gain-locked Raman fibre amplifier", *Opt. Commun.*, vol. 210, p. 57, 2002.

Chapter 4

High Power Continuous Wave Fiber Optical Parametric Oscillators (OPOs)

Using optical feedback, in principle any optical gain medium can be converted into an oscillator. When the gain is provided by a parametric process (superfluorescence), the result is known as an optical parametric oscillator (OPO). In earlier chapters we saw how a fiber OPA can provide large bandwidth and gain. If a fiber OPA is used as a gain medium, the oscillator is known as a fiber OPO. Much work has already been done on $\chi^{(2)}$-based OPOs [4.1][4.2][4.3][4.4]. They have already been in the market for a long time now. They can deliver hundreds of milliwats of average power, high conversion efficiency and enormous tuning ranges (from 500 nm to 2000 nm). On the other hand, there has not been much work done on fiber OPOs in the past. The reasons are high pump power requirements, and the existence of commercial $\chi^{(2)}$-based OPOs. But fiber OPOs have some added advantages such as all-fiber configuration, which is useful in telecommunication applications, pumping fiber Raman amplifiers, etc.

Fiber OPOs have been investigated in recent years, as they have the potential for providing tunable radiation in regions of the optical spectrum not well covered by the main laser systems. Most of the work has been performed with pulsed pumps, which can provide high peak powers, and hence lead to short OPOs that can be made from relatively lossy fibers, such as microstructured fibers. Powers obtainable with continuous-wave (CW) pumps are lower, and so larger lengths of low-loss fibers are

required. This limits performance, compared to pulsed pumps, and as a result few CW fiber OPOs have been investigated [4.5][4.6][4.7][4.8][4.9][4.10]

With the availability of HNLF, continuous-wave (CW) fibers OPAs with very high gain (70 dB) have been reported [4.11]. Also, ultrawide tuning range fiber OPOs have been reported. Using a similarly configured fiber OPA as a gain medium for fiber OPO, very large tuning range and large output powers are possible. In this work, we have made fiber OPOs, optimizing both tuning range and output powers. We have been able to obtain the largest tuning range achieved with CW fiber OPOs so far, and also large output powers.

4.1 CW Fiber OPO Centred at 1561 nm

In this work, we have made fiber OPOs, centred at 1561 nm, optimizing both tuning bandwidth and output powers. We have been able to obtain the largest tuning range achieved with CW fiber OPOs so far, and also large output powers. In Section 4.1.1 we discuss briefly our gain medium, i.e. a fiber OPA, and how the Raman effect influences its gain shape. In Section 4.1.2 the equation for the threshold of fiber OPOs is introduced. Section 4.1.3 describes briefly the recent work done on fiber OPOs. Section 4.1.4 describes the experimental set-up for the fiber OPO. Section 4.1.5 contains the results. Section 4.1.6 contains the method to get a flattened OPO output. Section 4.17 discusses the output power and conversion efficiency. Section 4.18 describes the output linewidth measurements obtained directly by an OSA. Section 4.19 contains the linewidth measurement done using a heterodyne scheme. Section 4.10 contains discussion and conclusion of the work done.

4.1.1 Gain medium

In fiber OPOs, the gain medium is a fiber OPA. Figure 4.1 depicts the gain spectrum of a fiber OPA, obtained with 2-W of CW pump power, and 300 m of HNLF, which had a nonlinearity coefficient of about 15 $W^{-1}km^{-1}$, and zero dispersion wavelength at 1560 nm.

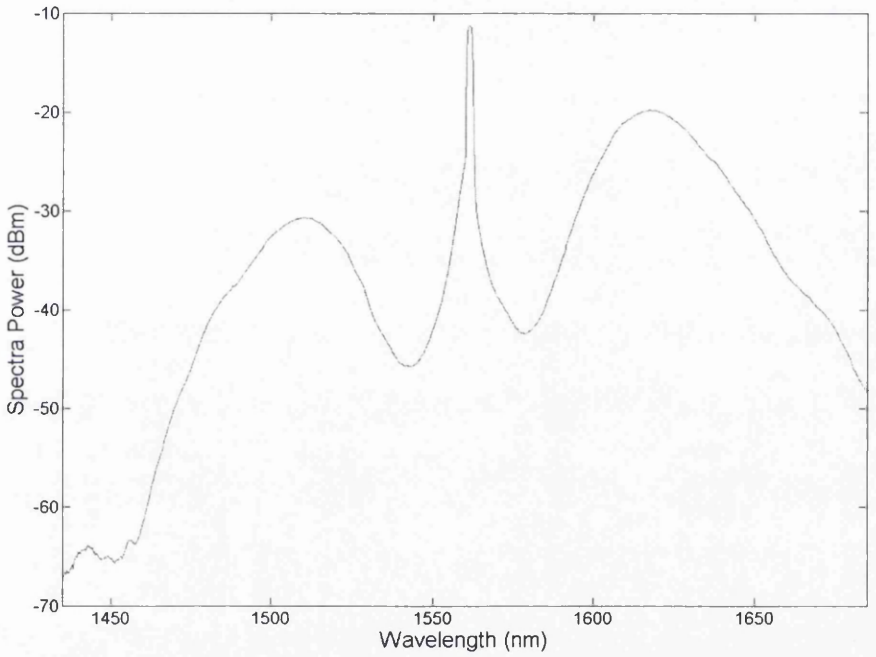

Fig. 4.1 Fiber OPA spectrum

We can see that there is large power asymmetry between the Stokes side and anti-Stokes side. This asymmetry can be attributed to Raman gain on the Stokes side, while the anti-Stokes side suffers from Raman loss. The combined effects of Raman and parametric gain were considered by A. S. Y. Hsieh et al. [4.12], and it was shown that phase-matched parametric gain also depends strongly on the real part of the Raman susceptibility. The measured real and imaginary parts of the Raman susceptibility versus frequency de-tuning are shown in Fig. 4.2. It can be stated that

up to 10 THz of frequency detuning, the real part dominates, while after 10 THz the imaginary part dominates.

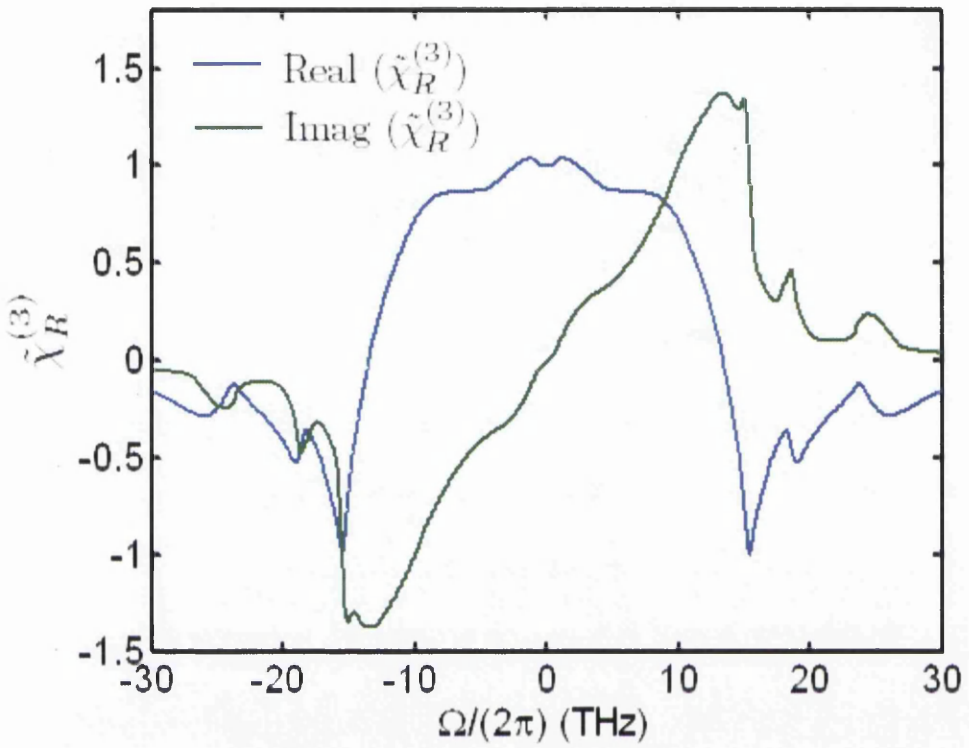

Fig. 4.2 Plot of both real and imaginary parts of the Raman susceptibility versus the frequency detuning [4.12].

4.1.2 Threshold pump power for fiber OPOs

The combined effects of Raman and parametric gain were presented in Ref. [4.12].

The combined gain can be written as:

$$G = \left|\cosh(\gamma RPL) \pm \frac{i(K-q)}{R}\sinh(\gamma PRL)\right|^2 \qquad [4.1]$$

where: $R = \sqrt{K(2q-K)}$; K is the phase mismatch wave vector; $q(\Omega) \equiv 1 - f + f\chi_R^{(3)}(-\Omega)$; f is the fractional strength of the Raman contribution; $\chi_R^{(3)}$ is the Raman susceptibility which includes both real and imaginary parts; Ω is the angular frequency detuning from the pump; γ is the fiber nonlinearity coefficient; P is the pump power; L is the fiber length. The Raman contribution gives asymmetry to the gain curve. For optimal phase matching, K = 1, and using a binomial expansion, $\sqrt{2q-1} = q$, leading to $R = q$. In the high gain limit, $\gamma PL >> 1$, and Eq. (1) reduces to:

$$G = \frac{1}{4}\left|1 \pm \frac{i(1-q)}{q}\right|^2 \exp(2\gamma P \,\mathrm{Re}(q) L). \qquad [4.2]$$

Introducing the transmissivity α of the cavity, the threshold condition becomes,

$$\alpha G = 1. \qquad [4.3]$$

For our cavity α = 0.1 near 1480 nm, and so more than 10 dB of gain is required for oscillation to take place. According to Ref. [4.9], the thresholds become similar for anti-Stokes and Stokes waves if the transmissivity (and Q-factor) of the cavity is small. Because of the Raman contribution the gain was higher on the Stokes side, but since our cavity has a low Q-value, thresholds for both Stokes and anti-Stokes sides could be assumed to be similar, and so we resonated the cavity on the anti-Stokes side.

4.1.3 Recent work done on CW fiber OPOs

The latest work on CW fiber OPO that has been published is from Auckland group [4.9]. They used 5 watts of CW pump power, and 500 m of dispersion shifted fiber (DSF), which had a nonlinearity coefficient of about 2.5 $W^{-1}km^{-1}$. They achieved 240 nm of bandwidth centred at 1550 nm, shown in Fig 4.3. The output linewidth was measured about to be 1-2 nm. They obtained external conversion efficiency (ECE) of nearly 2.5%. The reason for this low ECE is the very low output coupling fraction. Since this work was focussed on achieving an ultrawide tuning range, they minimized every loss in the cavity, including that due to output coupling.

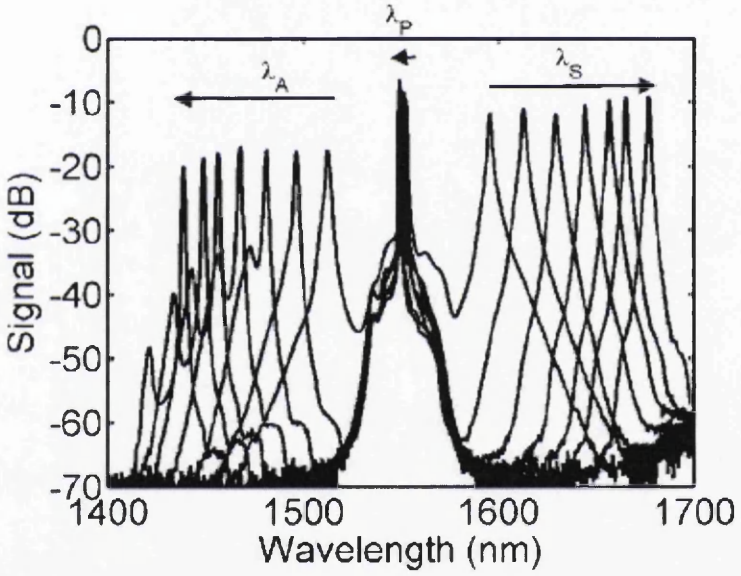

Fig. 4.3 Fiber OPO spectra in [4.9]

To the best of our knowledge, no work in CW fiber OPO has been done till date that gives not only ultrawide bandwidth but also very high output powers, leading to very large external conversion efficiencies. Here, we report two such CW fiber OPOs. The first one has a bandwidth of 211 nm, centred at 1560 nm, with watt-level output

power at long wavelengths (1600-1670 nm). This gave us a maximum external conversion efficiency of 61%. The other one gave us a record tuning range (254 nm) when we used only 1% output coupling, beating the previous one by a short margin of 14 nm. But as we discussed, our focus here was on output powers, so when we replaced the 1% output coupling by 50%, we got large output powers, leading to ECE as high as 30%, while still maintaining a large tuning range (242 nm.)

4.1.4 Experimental setup

The experimental setup is shown in Fig. 4.4. A tunable laser source was used as pump at 1561.5 nm. The pump light was phase-modulated by a 10 Gb/s PRBS source, to suppress the SBS. After this a 3-W EDFA was used in order to boost the pump power, followed by a 1 nm bandwidth filter to filter out the ASE. Then a wideband WDM coupler (1480/1550) was used to couple with low loss pump and intracavity signal into a 340-m long HNLF. The HNLF had a nonlinear coefficient γ = 15 $W^{-1}km^{-1}$, and ZDWL at 1560 nm. After it a 20-dB coupler was used to measure the SBS power, and input power to the HNLF, which was 33 dBm. After the HNLF a 3-dB coupler was used to couple half of the power out of the resonator, and to couple the other half back into it. Then in the resonator a narrow TBPF was used, which had an insertion loss of 5 dB, and a tuning range extending from 1460 to 1575 nm, i.e. primarily to the short-wavelength side of the pump. After TBPF, we used a PC in the cavity to maximize the output powers on the idler side. Total cavity loss was measured to be 9.8 dB.

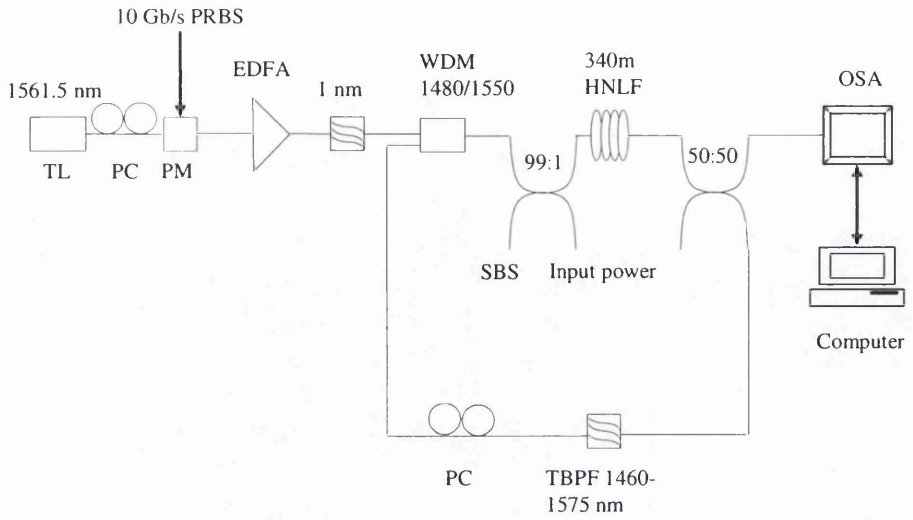

Fig.4.4 Experimental set-up for the fiber OPO

4.1.5 Results

To get the OPO to oscillate, the OPA open-loop gain for the signal must be higher than the intacavity losses. With the pump power injected into the OPA the maximum parametric gain was of the order of 50 dB, and so oscillation could readily be obtained upon closing the loop.

Figure 4.5 shows OPO output spectra obtained for various settings of the intracavity tunable filter. This shows that OPO lasing could be obtained from 1463 to 1674 nm, which corresponds to a 211-nm wide tuning range. The peaks on the anti-Stokes side of the pump correspond to light passing through the filter, which we call the signal; the peaks on the Stokes side are the corresponding idlers. The peak output power variation with signal wavelength is shown in Fig. 4.5. This shows an output power in the vicinity of 1 W from 1600-1670 nm. Peak powers on the Stokes

side are as much as 7.1 dB higher than the pump output power, which indicates strong pump depletion, and hence high external conversion efficiency (ECE).

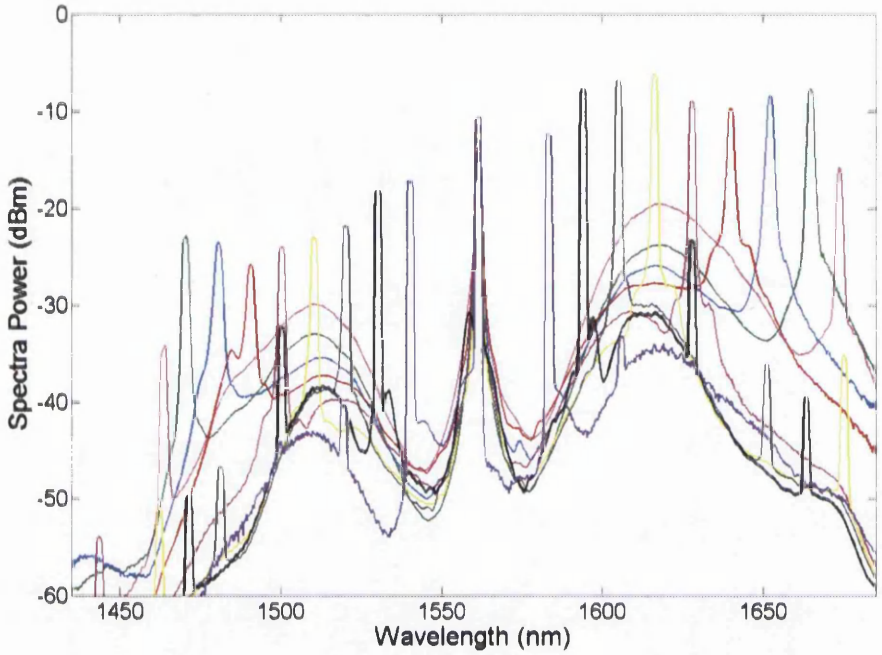

Fig. 4.5 Fiber OPO spectra obtained by selecting different wavelengths by TBPF.

4.1.6 OPO spectra with variable coupler to level the idler spectra

As we saw the Raman contribution at high pump powers renders the parametric gain asymmetric. For this reason, the peaks OPO outputs on both sides are unequal. This is a potentially undesirable feature of this OPO. To counter this problem, we used variable output coupling. Figure 4.6 shows the OPO spectrum achieved with variable output coupling. It can be seen that the amplitudes of the idler peaks are much more even this way. But the only variable output coupler that we had in our laboratory had an insertion loss varying in a nonlinear manner in terms of wavelength; it also had some insertion loss (1.5 dB). So we did not pursue this

technique further. But this data proves that if a variable coupler is used, a flatter output spectrum can be achieved.

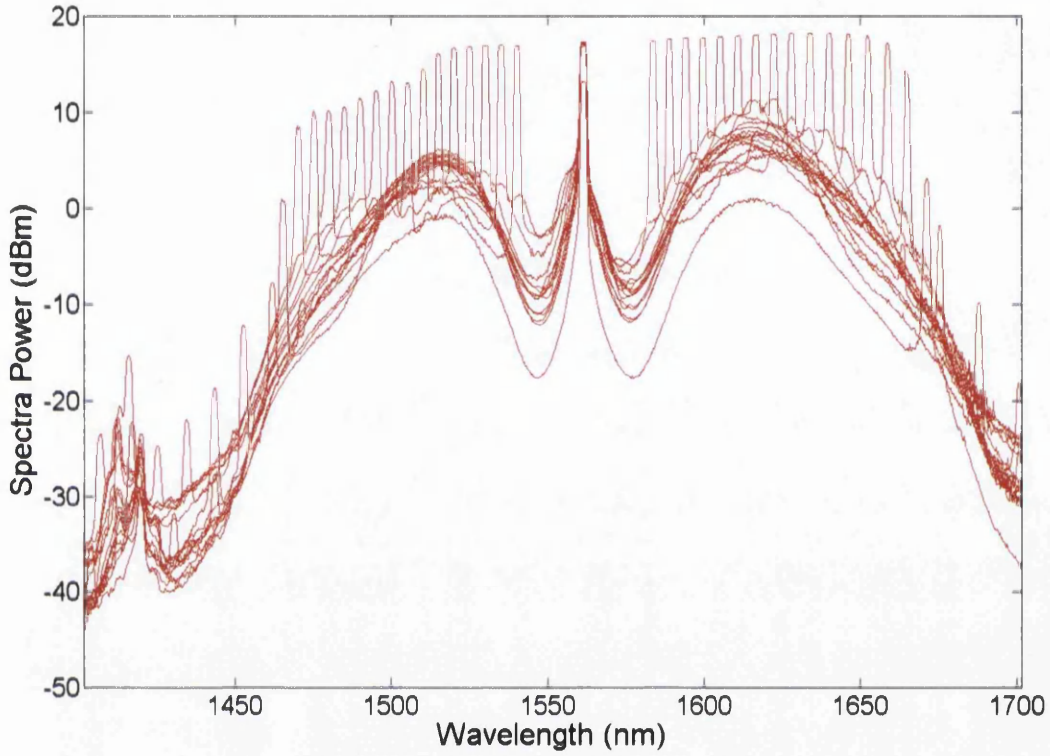

Fig. 4.6 Fiber OPO spectra obtained using variable output coupling.

4.1.7 Measurement of output power and external conversion efficiency

We defined ECE as the ratio of output power and pump power launched into the HNLF. Fig. 4.7 also shows the output ECE variation with wavelength, which reaches as high as 61 %. This is much higher than achieved in previous work [4.9]: the output ECE in the most recent work, Ref. 4.6, is only about 2.5 %. This is to our knowledge the best output ECE achieved to date with such a large tuning range. So, we achieved a tuning range comparable to the maximum achieved so far [4.6], but with higher ECE and output power.

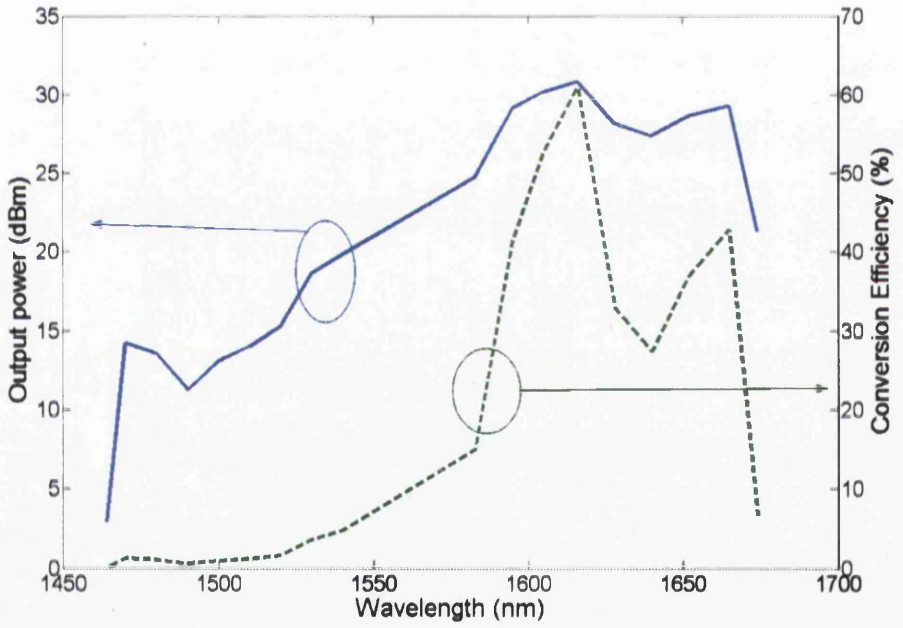

Fig 4.7 Output power and external conversion efficiency vs wavelength.

4.1.8 Linewidth measurements with a high-resolution OSA

Our OPO output spectra are narrower than in [4.9], as we used a narrower intracavity filter (0.25 nm FWHM). Figure 4.8 shows typical signal and idler output spectra, obtained for several values of the pump power near its maximum. We note that the idler peak power increases monotonically with the pump power, but that the signal power is maximum at the intermediate pump power. This may be due to the fact that at higher power, the Raman influence becomes even more prominent. This introduces further losses on the signal side. Another difference is that signal and idler have rather different spectral shapes. Looking at the 3-dB bandwidths, we see that the signal (idler) has about a 0.1 (0.2) nm linewidth. For these measurements, the resolution of the OSA was kept at its highest value (0.06 nm).

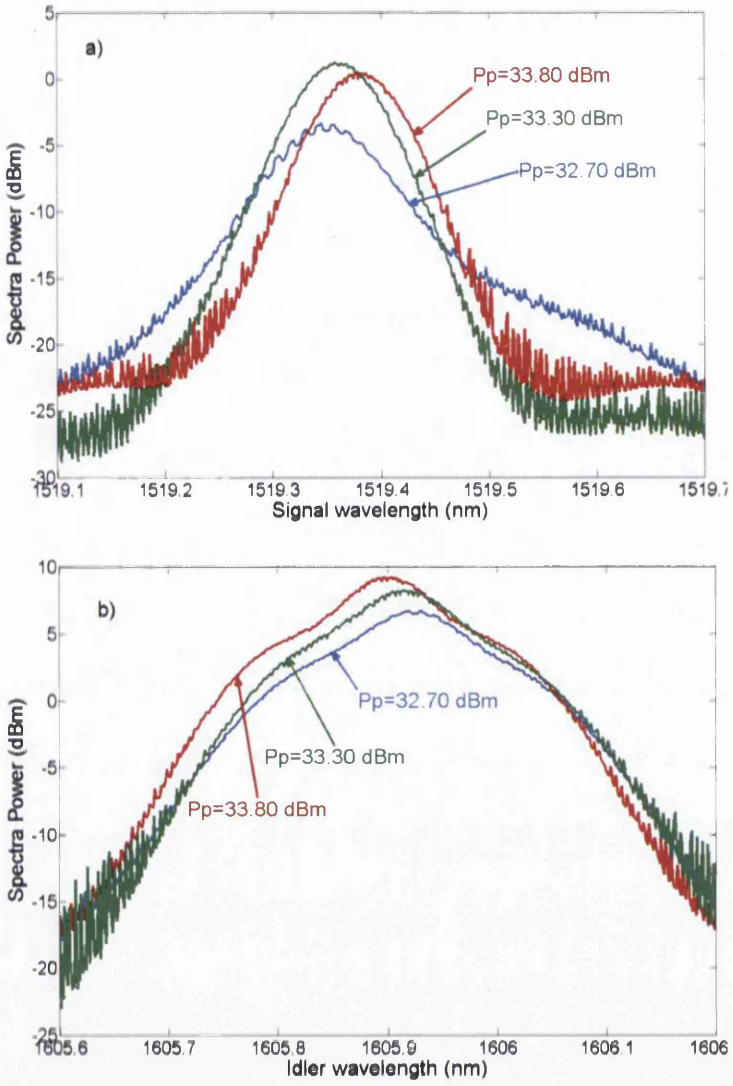

Fig. 4.8 Signal output spectra at different pump wavelengths (a); and idler output spectra at different pump wavelengths (b).

Actually, considering the fact that the OSA has a 0.06 nm resolution, we see that the signal is considerably narrower than the idler. In fact we have also measured the signal spectrum by heterodyne with a narrow-linewidth laser, and we found it to be about 10 GHz (0.08 nm), much narrower than the tunable filter itself (the electrical spectrum analyzer had a 250 ms sweep time). By contrast, even after deconvolving the OSA resolution, the accurate idler linewidth was found to be of the

order 0.15 nm. The difference in the linewidths can be understood as follows. The signal spectrum is forced to fit within the filter bandwidth, and so is necessarily narrow; but the idler spectrum is broadened during the parametric amplification, and acquires about twice the pump linewidth. The 20-dB linewidths are considerably larger, being of the order of 0.3 (0.5) nm for the signal (idler).

4.1.9 Linewidth measurement using heterodyne method

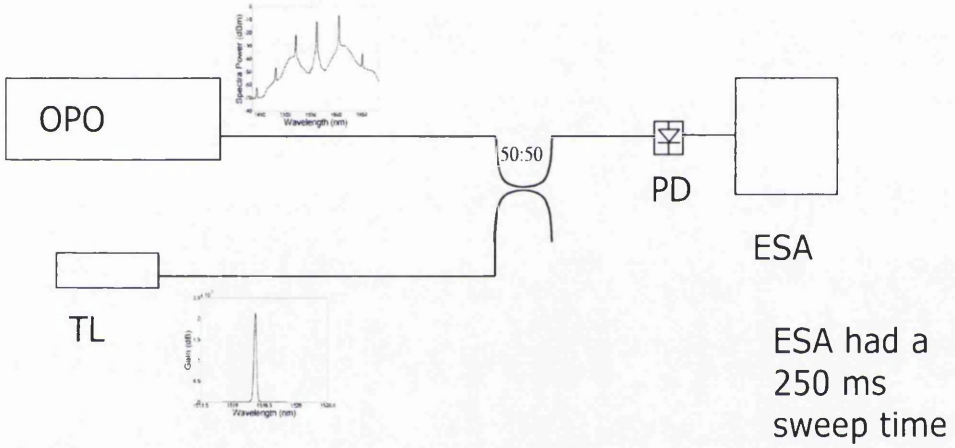

Fig. 4.9 Heterodyne set-up to measure the linewidth of the OPO ouput

Figure 4.9 shows the experimental set-up for the heterodyne technique to measure the OPO output linewidth. The OPO ouput was combined with the output of a narrow linewidth (few MHz) tunable laser (TL). TL was scanned to find the beat signal of signal and idler. The sum of the two was then detected by a photo-diode (PD). Its output then went to an electrical spectrum analyser (ESA). We used the fastest available sweep time of the ESA (250 ms).

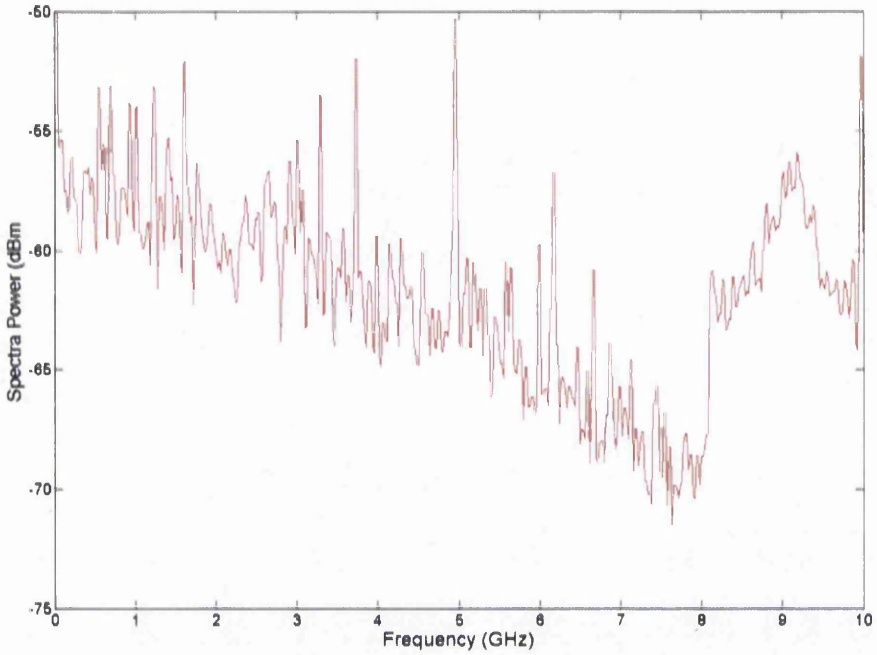

Fig. 4.10 Signal spectrum observed at the ESA

Figure 4.10 depicts the signal spectrum observed on the ESA. Signal linewidth is measured to be about 8 GHz, which matches well with that measured on the OSA, using deconvolution.

4.1.10 Discussion

We have shown that by using a 3-dB output coupler for extracting power from a fiber OPO, we can obtain over 1 watt of output power and 61 % external conversion efficiency at long wavelengths (1600-1670 nm), together with a tuning range over 200 nm. The 3-dB signal linewidth is as small as 0.08 nm. This kind of light source at long wavelengths is very rare, and it could find many applications, for instance: pumps for Raman amplifiers: large seed signals for Raman amplification; optical communication; gas detection, etc.

To exploit the fact that the fiber OPA bandwidth depends on the dispersion parameters and ZDW of the fiber used, we then used a fiber with a ZDW near 1600 nm to build a second fiber OPO. ZDWL closer to 1600 nm gave us gain beyond 1700 nm. When we reduced various losses, such as that due to ouput coupling, record tuning range (254 nm) was achieved. Also, when the output coupling was changed to 50%, we obtained very large output powers, and very high ECEs.

4.2 CW fiber OPO centred at 1593 nm

As we discussed in the previous section, we also assembled another fiber OPO, with different zero dispersion wavelength to extend the idler ouput beyond 1700 nm. The summary of the chapter is as follows: Section 4.2.1 states the gain medium for this work. Section 4.2.2 describes the experimental set-up. Section 4.2.3 contains all the results. And in section 4.2.4 we discuss and conclude the chapter

4.2.1 Gain medium

For this fiber OPO, we used 3 watts of CW pump power, 520 m of HNLF, which had a zero dispersion wavelength of 1592.9 nm, and nonlinear coefficient of about 15 $W^{-1}km^{-1}$.

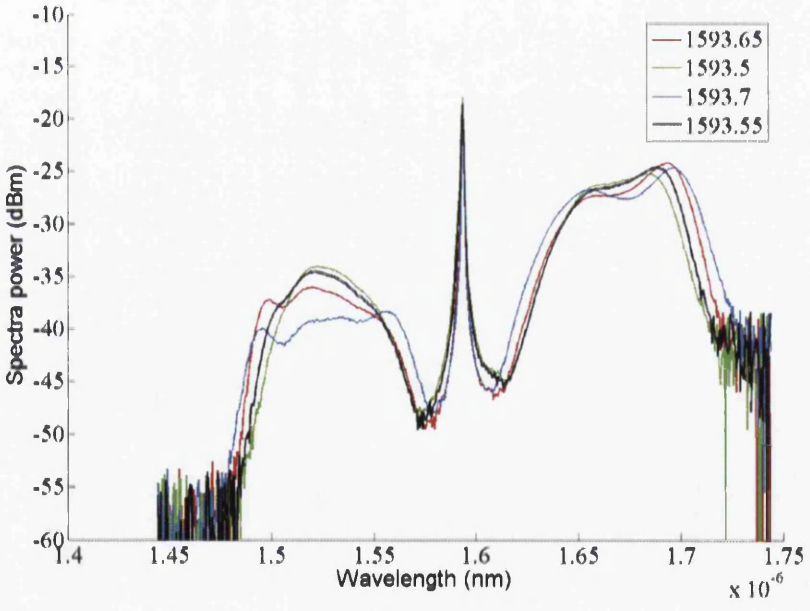

Fig. 4.11 OPA spectra at different pump wavelengths

Figure 4.11 shows the different fiber OPA ASE spectra obtained with different pump wavelengths (recorded with the feedback loop open). The red color corresponds to the 1593.65 nm pump wavelength, and it gives optimum bandwidth and gain to obtain tunability over more than 250 nm. The asymmetry in the OPA ASE spectra can be attributed to the Raman gain contribution. In order to make the OPO oscillate the gain should be higher than the losses in the ring (9.8 dB). The lowest signal wavelength where the signal gain was more than 9.8 dB was at 1476 nm, which corresponded to an idler at 1730 nm, giving us a total tuning range of 254 nm. (The OPA gain was measured by amplifying a tunable narrowband signal laser.)

4.2.2 Experimental Setup

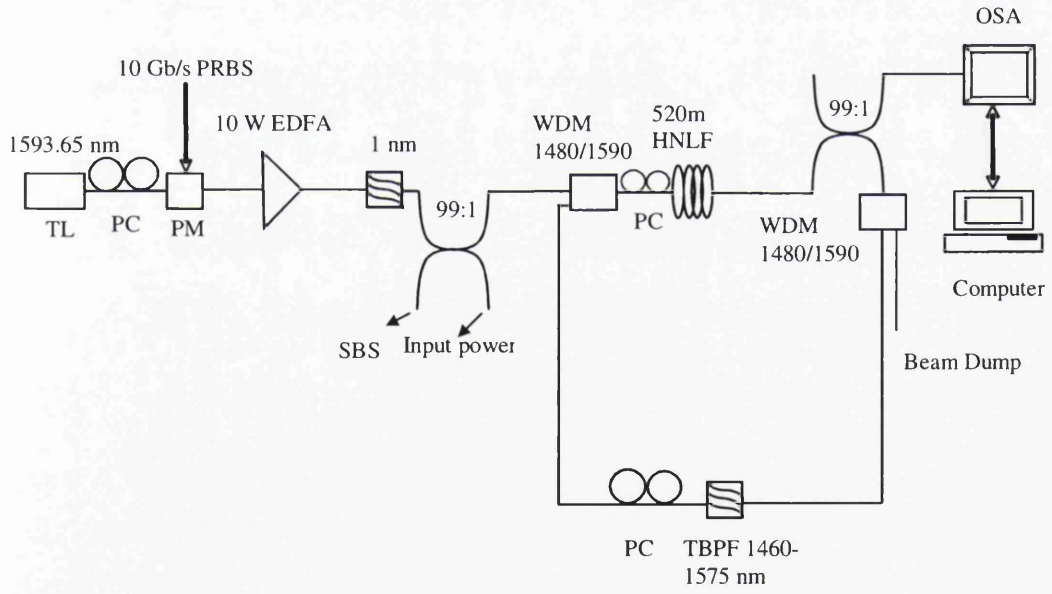

Fig. 4.12 Experimental set-up for fiber OPO.

The experimental setup is shown in Fig. 4.12. A tunable laser source at 1593.65 nm was used as pump. The pump light was then passed through a PC, and PM to be phase-modulated by a 10 Gb/s PRBS, to suppress SBS. After this a 10-W EDFA was used in order to boost the pump power. It was followed by a 1-nm bandwidth filter to remove the EDFA ASE. After this a 20-dB coupler was used to measure the SBS power and the input power to the HNLF, which was about 3 W (35 dBm). The SBS-reflected pump light level was up to 18 dBm. Then a wideband WDM coupler (1480 nm/1590 nm) was used to couple with low loss pump and intracavity signal into a 520-m HNLF. Before the HNLF, we used another PC to obtain different shapes for the OPA gain spectra, in order to maximize the gain at the desired wavelengths. The HNLF had the following parameters: nonlinearity coefficient γ = 15 W^{-1} km^{-1}; ZDWL at 1592.9 nm; fourth-order dispersion coefficient β_4 = 3×10^{-5} ps^4 km^{-1}; dispersion slope $D_\lambda = 0.025$ ps nm^{-2} km^{-1}.

The OPO output coupler was placed after the HNLF. We initially used a 20-dB coupler in order to minimize the loop loss, so as to maximize the OPA gain bandwidth, and therefore the tuning range. (Later on we replaced the output coupler by a 3-dB coupler in order to increase the output power, at the expense of a slightly reduced tuning range). The 20-dB coupler coupled 1% of the power out of the resonator, and the other 99% was coupled back into it. We then inserted a 1480 nm/1590 nm WDM coupler to partially remove the pump power and prevent damage to the intracavity filter. In the resonator a narrowband TBPF was used, which had an insertion loss of 5 dB, and a tuning range extending from 1460 to 1575 nm. The TBPF had a 3-dB bandwidth of 0.3 nm, and a 20-dB bandwidth of 0.8 nm. It was followed by another PC to match the states of polarization (SOPs) of the signal and the pump.

Total cavity loss was measured to be 9.8 dB in the 1480-nm signal wavelength region. The loss in the cavity was kept lowest near 1480 nm by using the WDM couplers, as the OPA gain was lowest near 1480 nm. But the loss in the cavity increased as the signal approached the pump, due to the WDM couplers. The main purpose of using a 1480 nm/1590 nm WDM coupler after the 20 dB coupler was to partially filter out the pump, so the power incident on the intracavity filter was below 1 W (damage threshold power). This increased the intracavity losses as the signal approached the pump, but the OPO still oscillated, as the gain in this region was quite high. The 1% power coupled out of the ring was fed into an OSA, which was connected to the computer by GPIB.

4.2.3 Results and discussions

Fig. 4.13 shows the fiber OPO spectra obtained for different settings of the intracavity filter. For each filter setting, there are two peaks: at the filter wavelength (signal), and at its symmetric with respect to the pump (idler). The right-hand side (idler) peaks have larger amplitudes, and this can be explained by the asymmetry of the fiber OPA ASE spectra due to the Raman contribution. The largest signal (filter) wavelength for which oscillation was obtained is 1575 nm. Oscillation could in principle be obtained closer to the pump, but our intracavity filter could not go beyond 1575 nm.

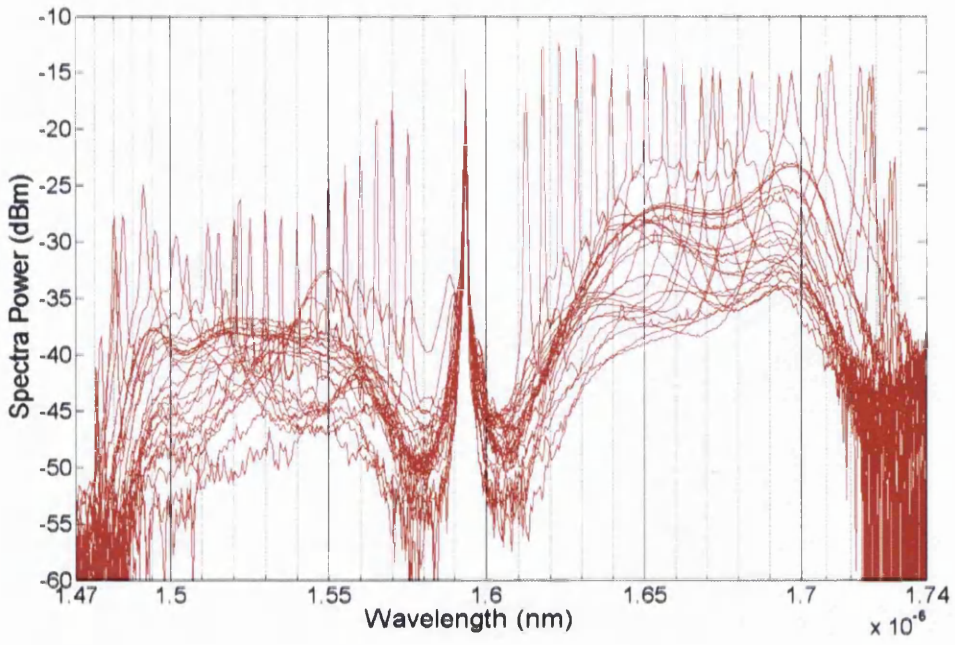

Fig. 4.13 Fiber OPO spectra, with a record tuning range of 254 nm.

To obtain large output powers, we then replaced the combination of 20 dB and 1480 nm/1590 nm WDM couplers by a 3 dB coupler. This increased the output powers, but it reduced the tuning range by a margin of 12 nm, as this slightly increased the loop losses.

Fig. 4.14 shows the resulting OPO spectra with a fixed input pump power of 34 dBm. The amplitudes of the peaks are saturated from 1670 nm to 1710 nm. This is because the gain is very high and intracavity loss is comparatively quite low. The idler peaks between 1670 nm and 1593 nm are not saturated because the cavity loss has gone up due the wavelength-dependent loss of the WDM couplers. Saturation effects in fiber OPAs have been observed [4.13]. The saturated gain can be written as [4.13]

$$G_{Ps} = \frac{G_0(\omega_s)}{1 + \frac{P_s}{P_{sat}}} \qquad [4.4]$$

P_{sat} is the saturation power defined as the input signal required to reduce the gain by 3-dB. G_0 is the low-power gain.

To avoid saturation, pump power should be adjusted. To maximize the output idler peaks, pump power was adjusted at every wavelength. This optimized pump power follows according to the losses in the cavity.

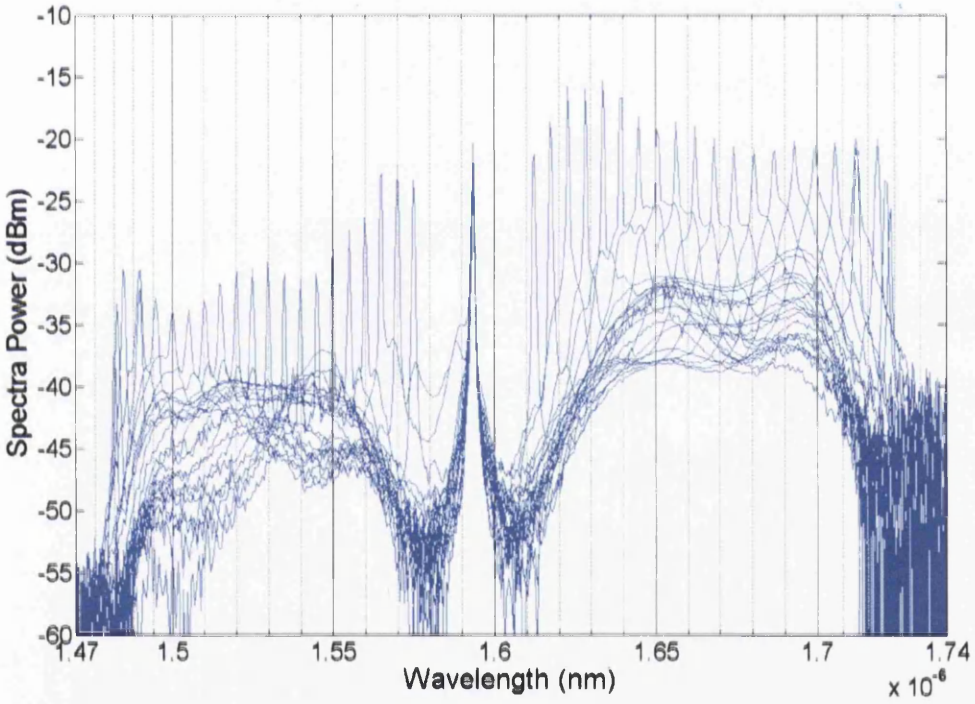

Fig. 4.14 Fiber OPO spectra with 50% output coupling.

Figure 4.15 plots the intracavity losses versus signal wavelength selected by the intracavity filter. To mitigate the saturation effects, pump power was optimized for each signal wavelength to obtain high signal and idler amplitudes. Figure 4.16 shows

the corresponding plot of optimized pump power versus signal wavelength. The step for pump power optimization was taken as 0.5 dB.

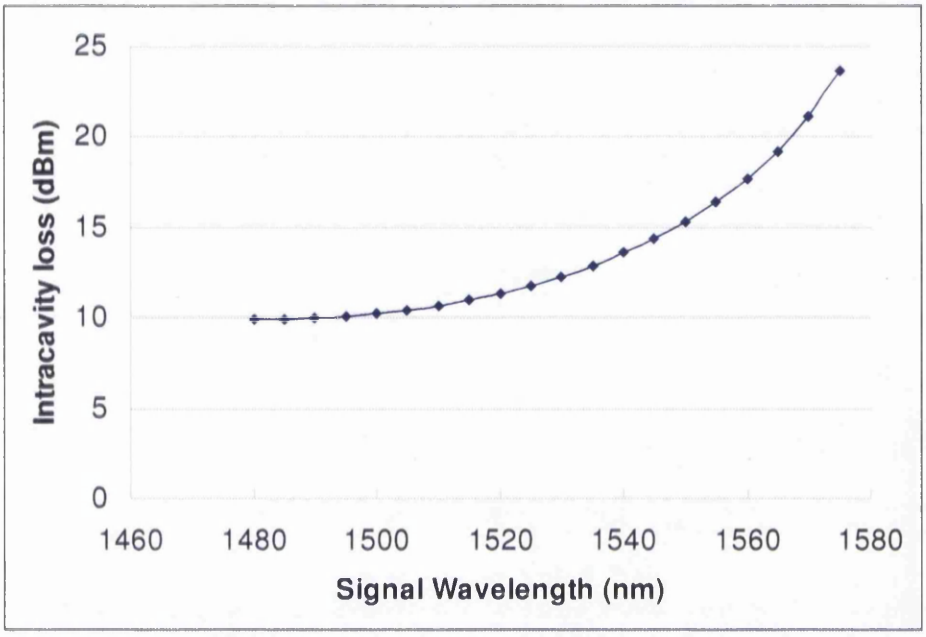

Fig. 4.15 Intracavity losses versus the signal wavelength.

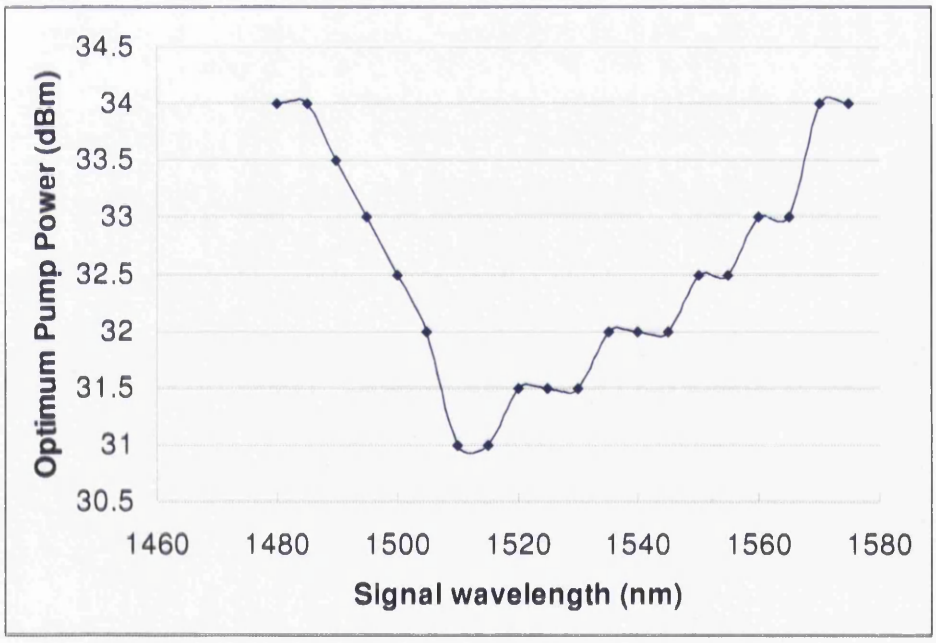

Fig. 4.16 Optimized pump power used versus the signal wavelength.

Fig. 4.17 shows the OPO spectra when the pump power was optimized for each setting of the intracavity filter. As can be seen from the comparison between Fig. 4.14 and Fig. 4.17, peaks in Fig. 4.17 from 1670 nm to 1710 nm are higher by 2-3 dB, which shows the benefit of the pump power optimization.

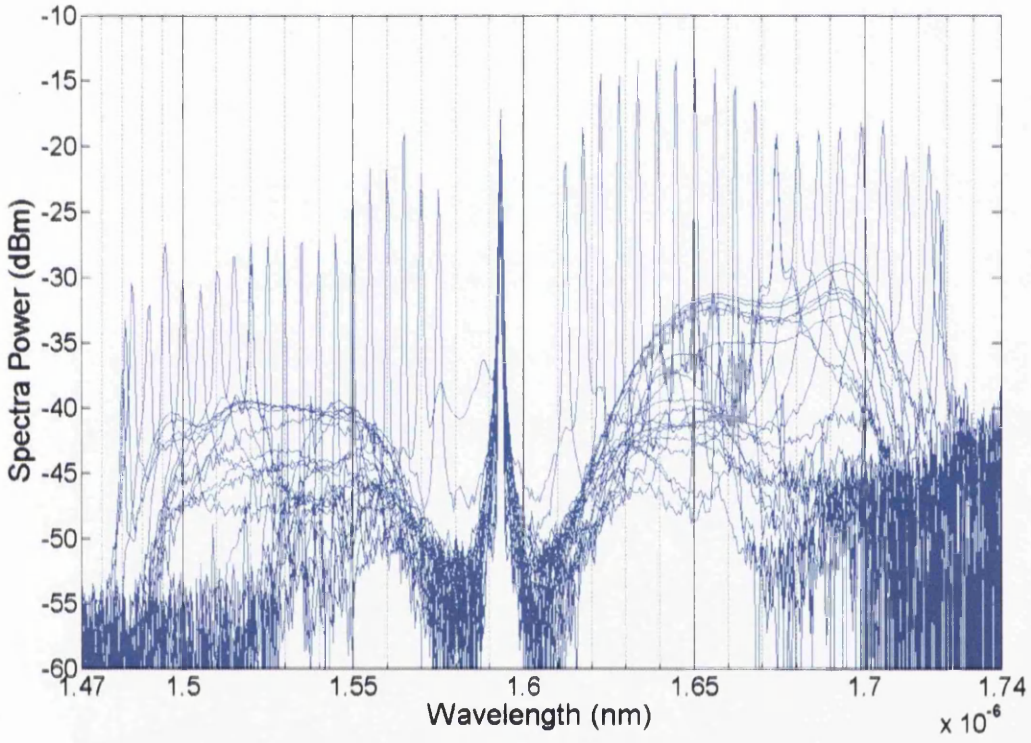

Fig. 4.17 Fiber OPO spectra obtained versus the variable pump power

Fig. 4.18 shows the plot of output power versus wavelength. Output powers are higher than 15 dBm from 1550 nm to 1720 nm, and higher than 20 dBm from 1615 nm to 1720 nm. (There was 40 dB attenuation between the OPO output and the OSA, in order to avoid damage to the OSA.)

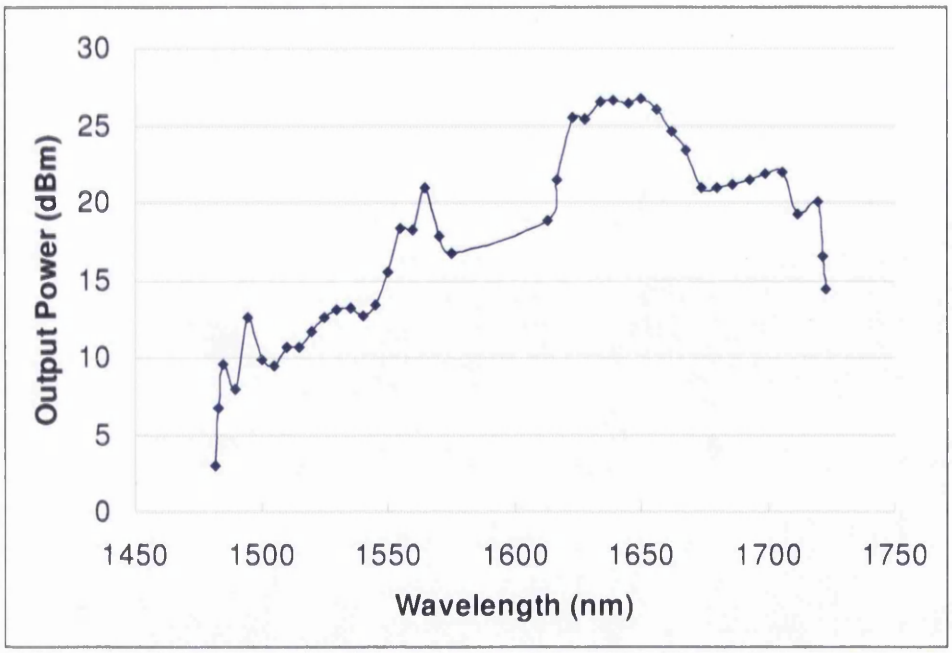

Fig. 4.18 Output powers obtained versus the signal wavelength selected by the TBPF, and its corresponding generated idler wavelength

4.2.4 Conclusion

We have operated a CW fiber OPO which has the largest tuning range demonstrated so far (254 nm), using less pump power than had been used to demonstrate previous large tuning range CW fiber OPOs. When output coupling is increased, the external conversion efficiency and output powers become quite large, still keeping the tuning range at near-record value (242 nm). This approach to fiber OPO design provides a powerful light source, tunable from 1610 to 1720 nm. Such a light source could be useful for remote sensing, optical communication, seeding Raman amplifiers, etc.

References

4.1 J. A. Giordmaine and R. C. Miller, "Tunable coherent parametric oscillation in $LiNbO_3$ at optical frequencies", *Phys. Rev. Lett.* vol. 14, p. 973, 1965.

4.2 L. E. Myers, R. C. Eckardt, M. M. Fejer, R. L. Byer, W. R. Bosenberg, and J. W. Pierce, "Quasi-phase-matched optical parametric oscillators in bulk periodically poled $LiNbO_3$," *J. Opt. Soc. Am. B* vol. 12, p. 2102, 1995

4.3 P. E. Powers, T. J. Kulp, and S. E. Bisson, "Continuous tuning of a continuous-wave periodically poled lithium niobate optical parametric oscillator by use of a fan-out grating design," *Opt. Lett.* vol. 23, p. 159, 1998

4.4 R. C. Eckardt, C. D. Nabors, W.J. Kozlovsky, and R.L. Byer, "Optical parametric oscillator frequency tuning and control," *J. Opt. Soc. Am. B,* vol. 8, p. 646, 1991

4.5 J. E. Sharping, "Microstructure Fiber Based Optical Parametric Oscillators," *J. Light-wave Technol.* vol. 26, p. 2184, 2008.

4.6 M. E. Marhic, K. K.-Y. Wong, L. G. Kazovsky, and T.-E. Tsai, "Continuous-wave fiber optical parametric oscillator," *Opt. Lett.* vol. 27, p. 1439, 2002.

4.7 C. J. S. de Matos, J. R. Taylor, and K. P. Hansen, "Continuous-wave, totally fiber integrated optical parametric oscillator using holey fiber," *Opt. Lett.* vol. 29, p. 983, 2004

4.8 Z. Luo, W.D. Zhong, M.Tang, Z. Cai, C. Ye, and X. Xiao, "Fiber-optic parametric amplifier and oscillator based on intracavity parametric pump technique," *Opt. Lett.* vol. 34, p. 214, 2009

4.9 Y. Q. Xu, S. G. Murdoch, R. Leonhardt, and J. D. Harvey, "Raman-assisted continuous-wave tunable all-fiber optical parametric oscillator," *J. Opt. Soc. Am. B* vol. 26, p. 1351, 2009

4.10 R. Malik and M.E.Marhic, "Tunable Continuous-Wave Fiber Optical Parametric Oscillator with 1 W Output Power," *In Optical Fiber Communication (OFC)/OSA' 2010*, paper JWA18 (March 21-25, San Diego, CA, USA).

4.11 T. Torounidis, P. A. Andrekson, and B.-E. Olsson, "Fiber optical parametric amplifier with 70-dB gain," *IEEE Photon. Technol. Lett.*, vol.18, p. 1194, 2006.

4.12 A. S. Y. Hsieh, G. K. L. Wong, S. G. Murdoch, S. Coen, F. Vanholsbeeck, R. Leonhardt, and J. D. Harvey, "Combined effect of Raman and parametric gain on single-pump parametric amplifiers," *Opt. Express* vol. 15, p. 8104, 2007

4.13 P. Kylemark, H. Sunnerud, M. Karlsson, and P. A. Andrekson, "Semi-Analytic saturation theory of fiber optical parametric amplifiers," *J. Light-wave Technol.* vol. 24, p. 3471, 2006.

Chapter 5

High output power fiber optical Raman amplifiers

5.1 Introduction

Most of the optical telecommunication systems operate in the C-band (1530-1560 nm), as silica-based fibers have lowest losses in this region [5.1]. However, the ever-increasing demand for larger data bandwidth motivates the search for amplifiers in other wavelength regions as well. As a result, erbium amplifiers in the L-band (1565-1625 nm) have also been developed [5.2][5.3].

Stimulated Raman scattering (SRS) can also provide amplification at any wavelength, if a suitable pump source is provided. For instance, Raman amplification in the U-band (1625-1675 nm) could easily be provided, as pump sources required for it need to be in the C- or L-band. EDFAs in these bands are commercially available, and can be used to provide high-power pumps. Spontaneous Raman scattering (SRS) was first observed by Sir CV Raman in 1928 in molecules,

for which he was awarded the Nobel Prize for Physics in 1930.

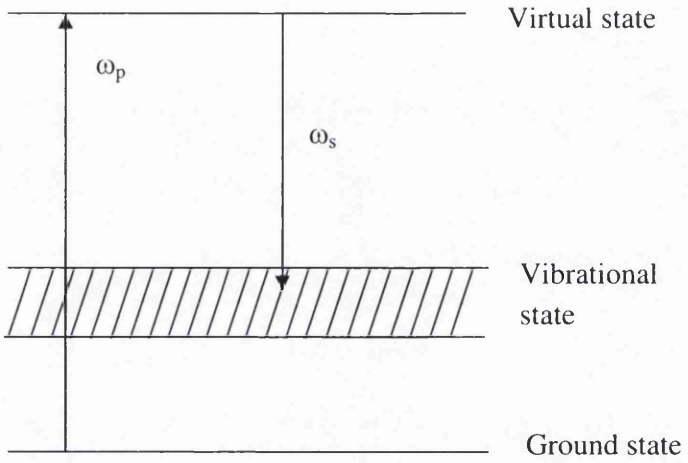

Fig. 5.1 Schematic illustration of Raman scattering process.

Figure 5.1 depicts the Raman scattering process from a quantum mechanical point of view. This process can be viewed as scattering of a photon of energy $h\omega_p$ by one of the molecules to a lower energy photon ($h\omega_s$). The incident pump light generates down-shifted radiation called the Stokes line. It also generates the up-shifted radiation called the anti-Stokes line. But the intensity of the anti-Stokes line is much weaker than that of Stokes line.

Stimulated Raman scattering was observed in fiber in the early 1970s, but back then it was only considered as a hindrance as it introduced crosstalk in multi-channel amplification systems. Now, with the availability of suitable pump sources, fiber Raman amplifiers have regained interest.

Fiber Raman amplification can be divided into two categories, distributed Raman amplification where the transmission fiber is itself used for Raman amplification, and discrete or lumped amplification, where a short piece of fiber is used for Raman amplification.

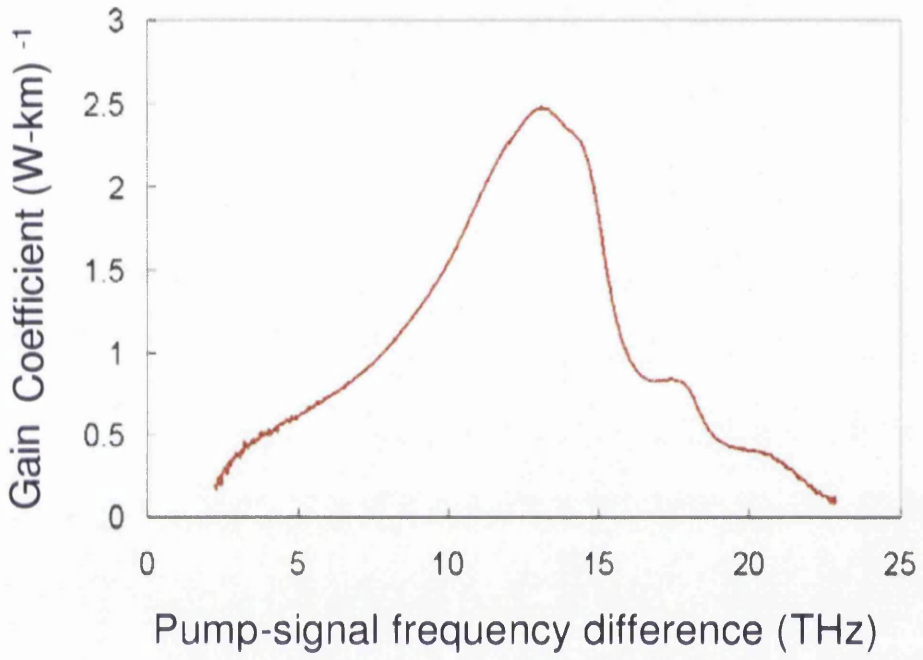

Fig. 5.2 Gain coefficient of an OFS Raman fiber vs. signal frequency detuning.

Figure 5.2 shows the Raman gain coefficient of an OFS Raman fiber versus the pump-signal frequency difference. The peak Raman gain coefficient occurs at about 12 THz signal-pump frequency difference. At 1550 nm, this corresponds to nearly 100 nm difference in terms of wavelength units. In this work, we have focussed on how to generate high CW output powers in the U-band.

Raman amplification in the U band has been reported with high gain (more than 30 dB) [5.4][5.5]. But since very low signal input power (-31 dBm) was used, output power was very low.

Since then CW fiber OPOs with watt-level output power in the U-band have been reported [5.6]. With the injection of a large seed, very high output powers can be achieved, using a hybrid approach of OPO and Raman amplification,

In this work, we have obtained more than 3 watts of output power from a Raman amplifier in the U-band. To obtain a large seed signal in the U-band, we have used a fiber OPO as the signal provider in the U-band. To our best of knowledge this is the first time that such high power generation has been reported in the U-band.

5.2 Large seed signal in U-band for Raman amplification

Lasers are not readily available in the U-band near 1650 nm, and the ones that are available do not have much output power. As high output power, widely tunable fiber OPOs have been reported [5.6][5.7], high output powers have been generated in entire U-band.

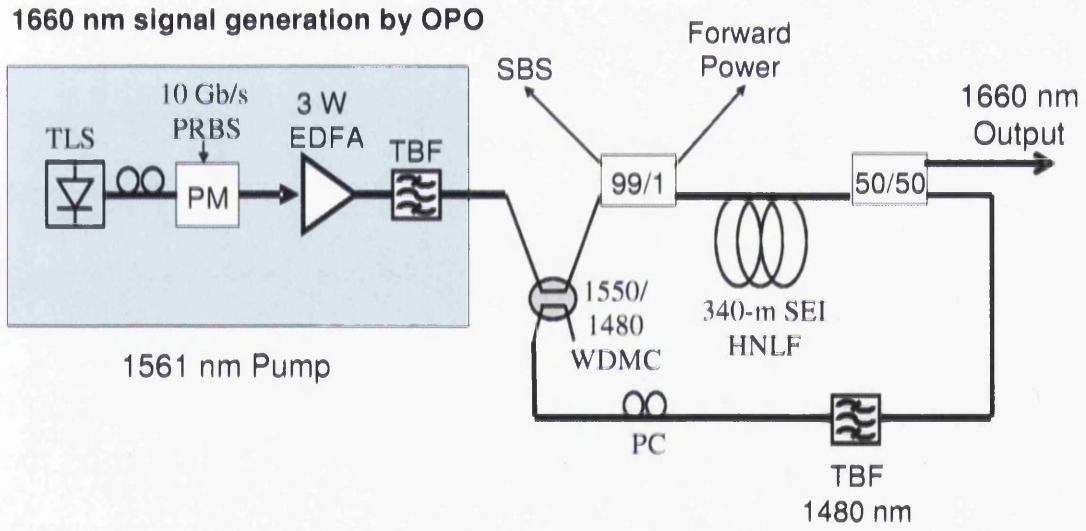

Fig. 5.3 Experimental set-up for fiber OPO to generate a large seed at 1660 nm.

Figure 5.3 shows the experimental set-up for a fiber OPO used to generate a large seed at 1660 nm. Tunable laser source (TLS) provided the pump at 1561.5 nm. The latter entered a PM driven by 10 Gb/s PRBS to suppress SBS. It was then followed by an EDFA to boost the pump. TBPF with linewidth of 1 nm was used to filter out the ASE generated by the EDFA. 340 m of HNLF was then used as a parametric gain medium, followed by a 3-dB coupler which couples half of the power into the cavity. In the cavity we had a TBPF to select the signal wavelength in the S-band, which generated the corresponding idler in the U-band. We used a PC in the cavity the match the SOPs of the signal and the pump to have maximum gain.

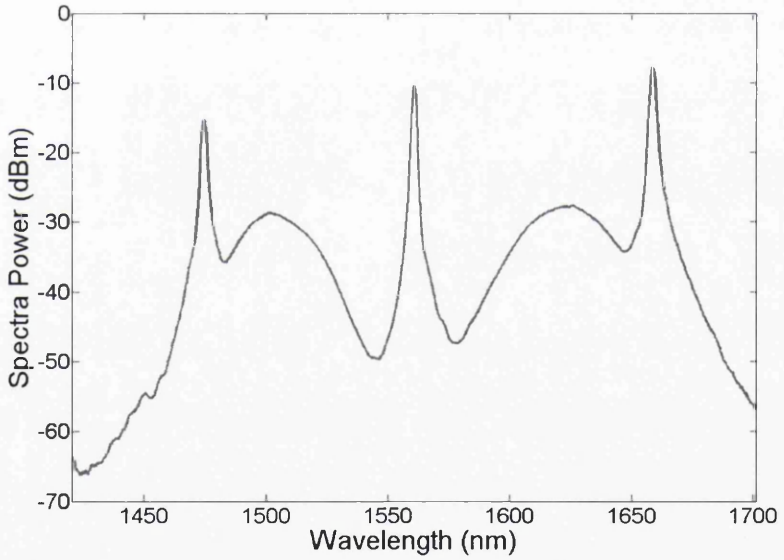

Fig. 5.4 Output near 1660 nm from the fiber OPO

Figure 5.4 shows the output of the fiber OPO with signal wavelength near 1480 nm and idler at 1660 nm. This output can be tuned using TBPF inside the cavity and selecting the different signal wavelengths.

5.3 Pumping source for Raman amplification

One hindrance with using high-power CW sources is backreflected light, mainly due to SBS. The SBS threshold depends on the linewidth of the pump source, and it can be increased by frequency/phase dithering (pump line width broadening) . The other way is to use some large-linewidth pump source. Commercial lasers have, in general, linewidths of the order of few MHz. We built an Erbium-doped fiber laser (EDFL) to provide a broad linewidth pump source.

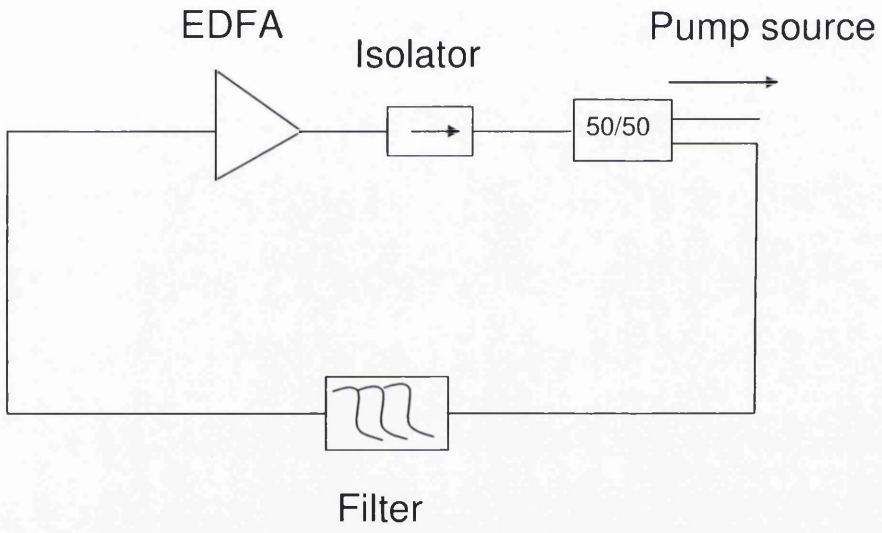

Fig. 5.5 EDFL set-up for broad linewidth pump source.

Figure 5.5 shows the set-up for the EDFL. We used an 18-dBm EDFA, followed by an optical isolator to prevent light going back to the EDFA. We then inserted a 3-dB coupler to couple half of the power back into the resonator, while coupling out the other half. We placed a TBPF (Santec-OTF 300) inside the cavity with a tuning range from 1530 nm to 1560 nm, and a bandwidth of about 0.3 nm.

Figure 5.6 shows the EDFL output obtained on OSA. Its linewidth is nearly 0.3 nm, which is same as that of the filter used for the EDFL.

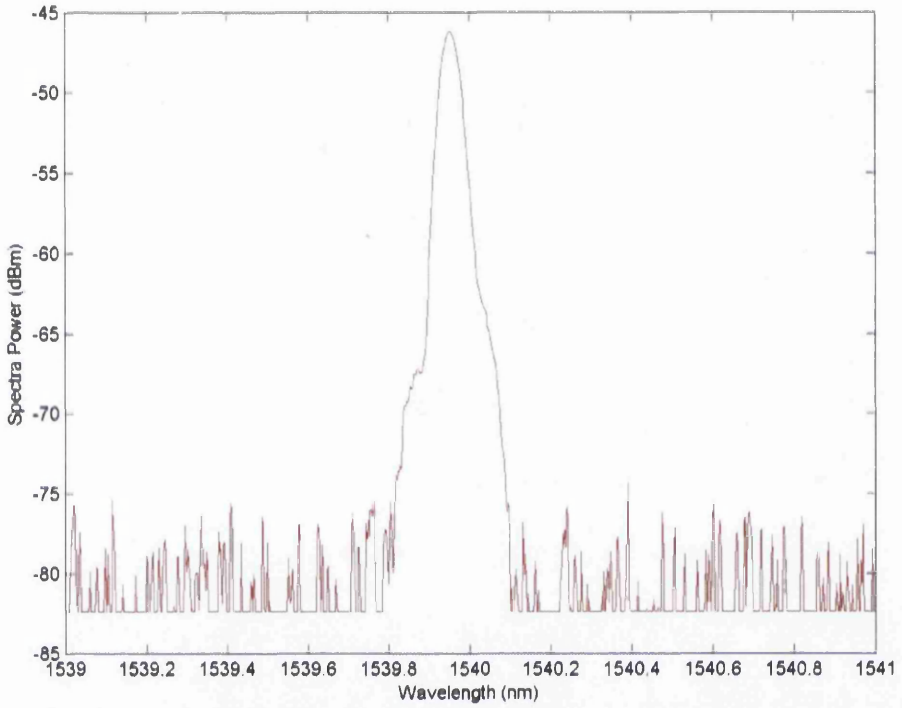

Fig. 5.6 EDFL output recorded on OSA.

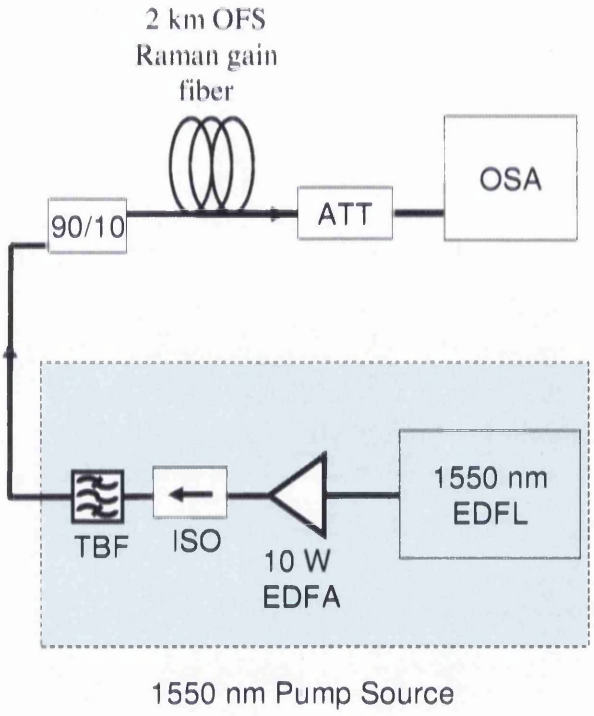

Fig. 5.7 Experimental set-up for Raman amplification

Figure 5.7 shows the experimental set-up for the fiber Raman amplifier. EDFL gives us the pump at 1550 nm. The latter is boosted by the 10-W EDFA, followed by the high-power optical isolator. A TBPF was used to filter out the ASE of the EDFA. It was followed by a 90/10 coupler, which coupled 90% of the pump into the 2-km long OFS Raman fiber, which had a Raman coefficient of about 2.5 $W^{-1}km^{-1}$, dispersion value of -20 ps/(nm km) at 1550 nm, and attenuation of about 0.3 dB/km. The output spectrum of the fiber was displayed by the OSA, after attenuating it.

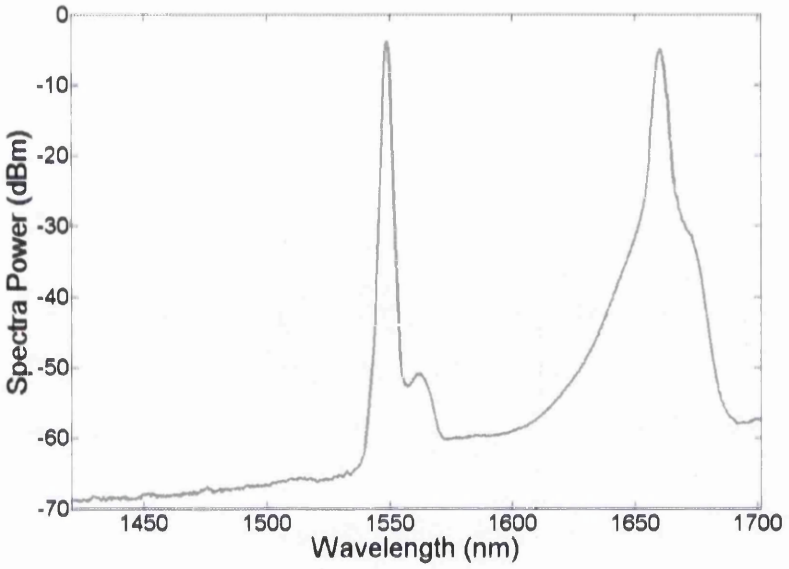

Fig. 5.8 Output showing Raman ASE near 1660 nm.

Figure 5.8 shows the output spectrum from the fiber Raman amplifier. The peak at 1550 nm depicts the pump. The peak near 1660 nm corresponds to ASE due to the Raman gain.

5.4 Hybrid experimental set-up containing fiber OPO and fiber Raman amplifier

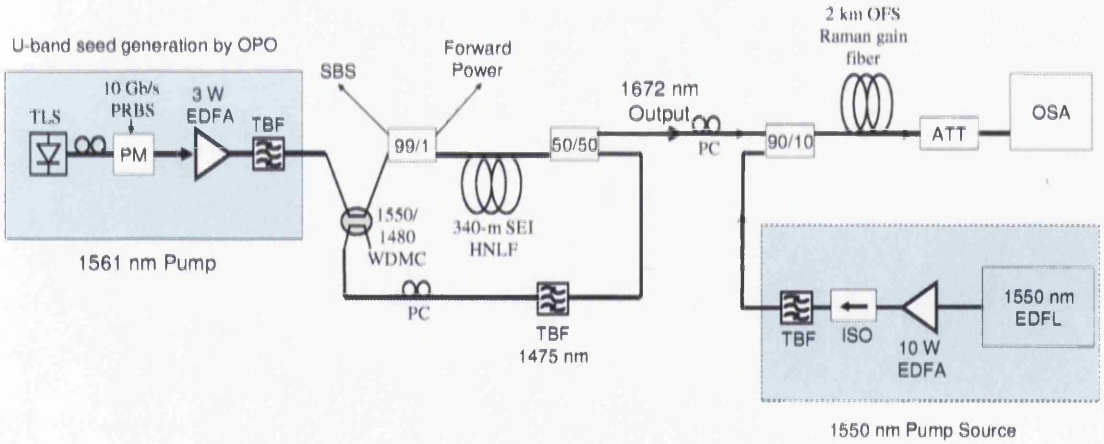

Fig. 5.9 Complete experimental set-up showing OPO seed used for Raman amplifier.

Figure 5.9 shows the experimental set-up for the hybrid structure with fiber OPO output serving as the seed for the fiber Raman amplifier. We have discussed this experimental set-up earlier. The 10% fiber OPO output goes through the 90/10 coupler into the Raman fiber.

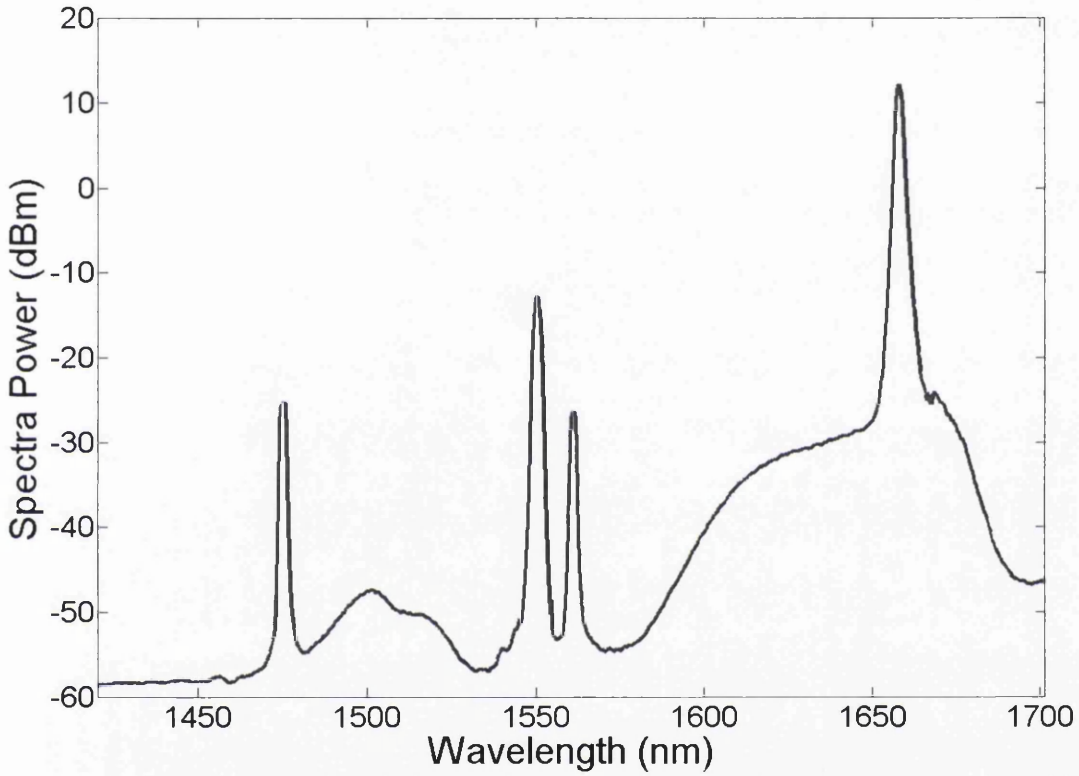

Fig. 5.10 Output spectra obtained at OSA.

Figure 5.10 shows the Raman amplifier output spectra resulting from seeding the fiber Raman amplifier with the OPO output. Both pumps, for the Raman amplifier and the OPO are almost 100% depleted. This is visible from the peak amplitudes in the spectrum. This indicates the excellent conversion efficiency achieved. The output peak power at 1660 nm was measured with an OSA resolution of 2 nm. The output power was measured to be 35 dBm (3 W).

5.5 Tunability

The tunability of the whole arrangement can be controlled by adjusting the Raman pump wavelength by using the TBPF inside the EDFL, and by adjusting the seed signal using the TBPF inside the fiber OPO.

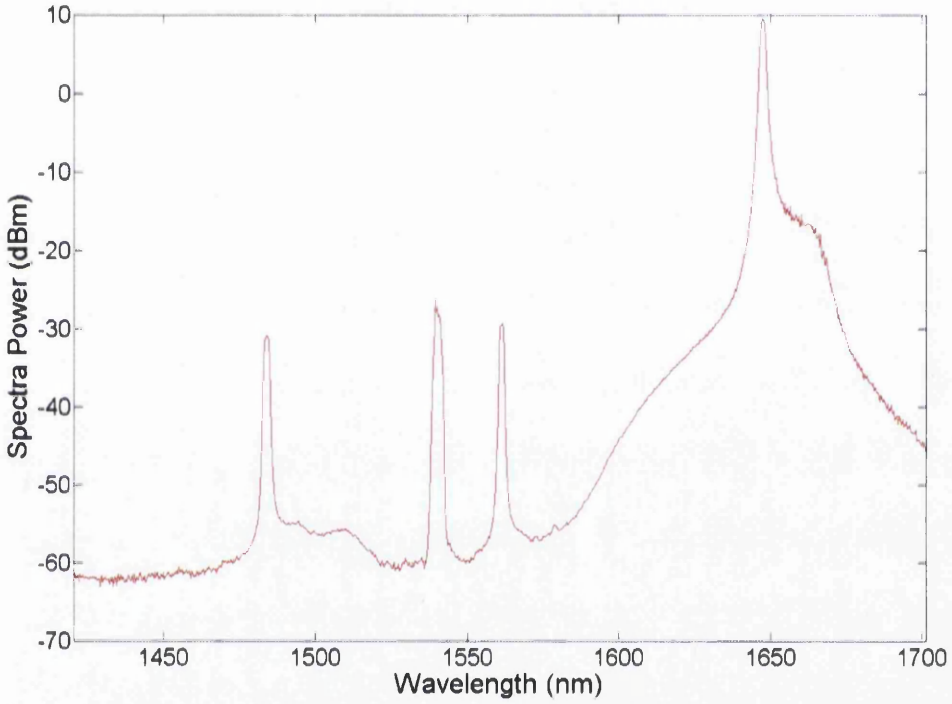

Fig. 5.11 Raman amplifier output spectrum measured by the OSA.

Figure 5.11 shows the Raman amplifier spectrum, for output generation at 1650 nm. It was obtained by changing the pump wavelength to 1540 nm. Similar output power was generated at this wavelength as at 1660 nm.

Conclusion

We have shown that by combining a high power tunable OPO and Raman amplification, 3 W of power can be generated over the whole U-band by using just 3

W of Raman pump power. The high output power is due to the use of high seed power, and near-complete depletion of the Raman pump. Such a powerful source of tunable U-band radiation could find applications in free-space optical communication, remote sensing, etc.

References

5.1 G. P Agrawal, "Nonlinear Fiber Optics", fourth edition, Academic Press, San Diego, USA, 2007.

5.2 H.S. Chung, M.S. Lee, D. Lee, N. Park and D.J. DiGiovanni, "Low noise, high efficiency L-band EDFA with 980nm pumping", *Electron. Lett.* vol. 35, p. 1099, 1999.

5.3 J. Lee, U. C. Ryu, S. J. Ahn, and N. Park, "Enhancement of Power Conversion Efficiency for an -Band EDFA with a Secondary Pumping Effect in the Unpumped EDF section", *IEEE Photon. Technol. Lett.* vol. 11, p. 42, 1999.

5.4 H. Masuda, S. Kawai, K.-I. Suzuki and K. Aida, "1.65pm band fibre Raman amplifer pumped spontaneous emission light source", *Electron Lett.* vol. 34, p. 2339, 1998.

5.5 P.C. Reeves-Hall, D.A. Chestnut, C.J.S. De Matos and J.R. Taylor, "Dual wavelength pumped L- and U-band Raman amplifier", *Electron. Lett.* vol. 37, p. 883, 2001.

5.6 R. Malik and M. E. Marhic, "Tunable Continuous-Wave Fiber Optical Parametric Oscillator with 1-W Output Power," *In Optical Fiber Communication (OFC)/OSA' 2010*, OSA Technical Digest (CD) (Optical Society of America, 2010), paper JWA18.

5.7 R. Malik and M. E. Marhic, "Continuous Wave Fiber Optical Parametric Oscillator with 254 nm Tuning Range," in *Latin America Optics and*

Photonics Conference, OSA Technical Digest (CD) (Optical Society of America, 2010), paper MD1.

Chapter 6

Design and realization of low-cost Multi-tone RF phase modulation for the suppression of stimulated Brillouin scattering

6.1 Introduction

SBS is a process in which, when a certain pump amplitude is reached, the pump power starts being reflected back into the nonlinear fiber. This process can be explained in terms of electrostriction [6.1], whereby the variations in the electric field of the pump produce acoustic vibrations in the medium. The pump beam then undergoes Brillouin scattering from these vibrations. The part of the pump that is reflected back is at different frequency (lower) than the forward travelling pump, and the difference between these two is called the Brillouin frequency shift. This shift is typically in the order of 10 GHz in silica-based fibers.

The expression for the Brillouin shift is given by [6.2]

$$\nu_b = \frac{2n_0 v_b}{\lambda} \qquad [6.1]$$

where n_0 is the refractive index, v_b is the velocity of sound waves, and λ is the wavelength of the pump light. The pump power at which a significant fraction starts being reflected back is known as the SBS threshold. It can be as low as 1 mW in a long fiber for a CW pump, or when pumping is in the form of relatively long pulses.

The SBS threshold for CW light can be examined using steady state conditions. It is given by

$$P_{cw} = 21\frac{A_e K}{g_B L_e} \quad , \qquad [6.2]$$

where L_e is the effective interaction length, given by

$$L_e = \frac{1-\exp(-\alpha l)}{\alpha} \quad . \qquad [6.3]$$

A_e is the effective core area of the fiber, α is its loss coefficient, l is its length , K is the polarization factor, and g_B is the peak Brillouin gain coefficient. K accounts for the polarization scrambling between pump and Stokes waves; for complete scrambling as in conventional single mode fibers, $K = 2$.

Equation [6.2] is valid only when the pump has a narrower linewidth than the Brillouin linewidth. For pump light with linewidth greater than the Brillouin linewidth, the SBS threshold is given by

$$P_{cw} = 21\frac{A_e K}{g_B L_e}\frac{\Delta\upsilon_P \otimes \Delta\upsilon_B}{\Delta\upsilon_B} \qquad [6.4]$$

Here, $\otimes$ denotes the width of the convolution of the pump spectrum and the Brillouin gain spectrum.

If SBS occurs, most of the input light will be reflected back to the input end of the fiber. This process may put severe restrictions on the amount of power we can launch into a fiber. So, it becomes necessary to suppress this effect.

6.2. Suppression of Stimulated Brillouin Scattering

Techniques for the suppression of SBS are quite well known. They include the creation of temperature and/or strain variations along the fiber [6.3][6.4], and broadening the pump spectra [6.5][6.6]. It is well known that the efficiency for SBS decreases as the linewidth of the optical source is increased. Consequently, artificial broadening of the spectrum of the optical source, such as accomplished with optical modulation, serves as a means of increasing the threshold for SBS. In particular, artificial pump broadening can be done by PRBS RF phase modulation or Multi-tone RF phase modulation. In this chapter e compare these two approaches.

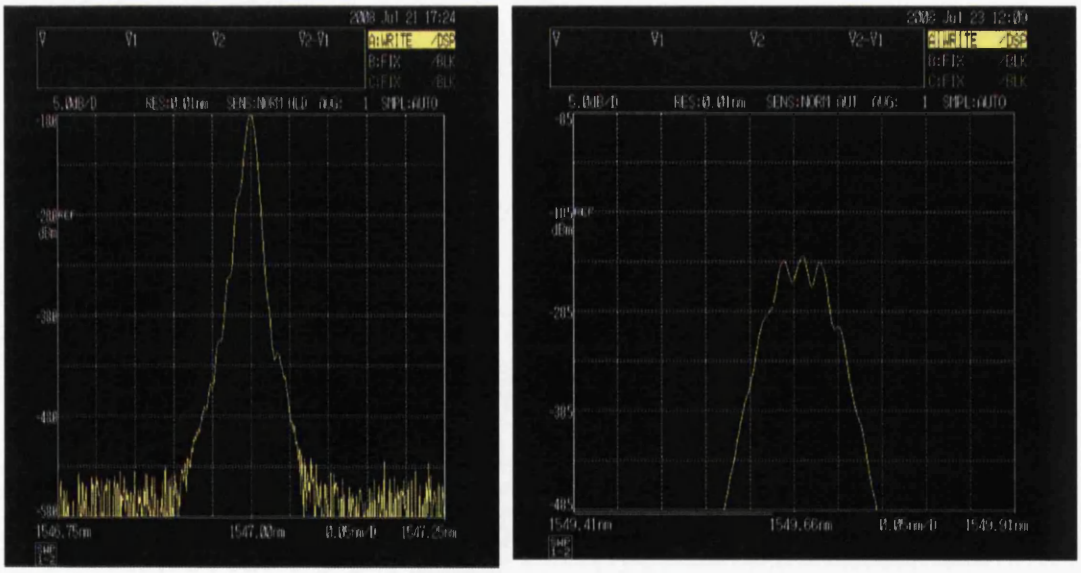

Fig 6.1 Optical spectra of a laser source: (left) no phase modulation; (right) after broadening by phase modulation

Figure 6.1 shows the spectra of a laser light and its broadening by phase modulation. We modulate its phase with a 2.5 GHz RF oscillator. The RF amplitude was adjusted to obtain three main peaks with approximately the same amplitude. As the peak spectral power is reduced by a factor of 3, the increase in SBS threshold is 5 dB.

We then designed an optimized Multi-tone RF modulation scheme and then built it ourselves.

6.3. Design of Phase Modulation Box

To modulate the phase of the laser, we built the phase modulation box based on Multi-tone RF phase modulation. The components that we used for building the box are as follows:

1) Four RF sinusoidal with frequency ranges (50-100) MHz, (200-380) MHz, (612-1200) MHz, and (2165-2650) MHz respectively.
2) Four RF attenuators with frequency range (10-2500)MHz
3) Connectors
4) 9 Potentiometers (0-50 K Ohm), and different resistors to provide the operating voltages (12 V for oscillators and 5 V for attenuators) and tuning voltages (0-18 V) for oscillators and attenuators.
5) 9 On/Off buttons for oscillators and attenuators
6) 1 main On/Off
7) Amplifier, with maximum gain of 28 dBm
8) AC to DC converter

We obtained a 19 V supply from an AC to DC converter. Then we built a circuit for supplying the required voltages to oscillators, attenuators, and 15 V amplifier. We assembled all the RF oscillators and attenuators using combiners and splitters. To optimize the technique, we equalized all four RF's power with the help of attenuators. The output from all the four RF oscillators goes to the amplifier. By using attenuators, we made sure that the output cannot exceed 0 dBm, the maximum input limit of the amplifiers. Then the output from the amplifier goes to the SMA connector port (output port of the box) to drive the phase modulator.

Table 6.1 shows the different components used in building the Multi-tone RF modulation box and its final form.

Part#	Piece Part Description	Qty	Vendors	Part #	Est $/unit	Total ($) Cost
1	DC Power Supplies (24V)	1	Sunpower	S-25-24	30	30.00
2	Variable Potentiometer (50KΩ)	9	Farnell UK	ETI - MW22B-10-50K	15	135.00
3	Resistor voltage divider	5				
4	Resistor voltage divider	5				
5	ON-OFF switches	5	Farnell UK	EN61058-1	8	40.00
6	Oscillator #1	1	minicircuit	ZX95-100+	38	38.00
7	Oscillator #2	1	minicircuit	Zx95-400+	40	40.00
8	Oscillator#3	1	minicircuit	Zx95-1200W+	50	50.00
9	Oscillator #4	1	minicircuit	ZX95-2650+	44	44.00
10	Adjustable Attenuator#1	1	minicircuit	ZX73-2500+	50	50.00
11	Adjustable Attenuator#2	1	minicircuit	ZX73-2500+	50	50.00
12	Adjustable Attenuator#3	1	minicircuit	ZX73-2500+	50	50.00
13	Adjustable Attenuator#4	1	minicircuit	ZX73-2500+	50	50.00
14	3 dB combiner/splitter	3	minicircuit	ZFSC-2-2650-S+	75	225.00
15	SMA connectors	7				
16	SMA semi rigid RF cable	8				
17	Broadband RF amplifier	1	Minicircuit	ZHL-42	895	895.00
18	Front panel SMA Bulk connector	1				
19	Power electrical plug back panel	1				
20	Front panel ON/OFF main power switch or DC power supply	1	Farnell UK	C1353AHNAA	5	5.00
21	Back panel electrical fuse	4				
22	Power electrical cable					
23	oscillator#5	1				
24	Back mount mechanical assemblies	1	Farnell UK		150	150.00
					Total	1,852.00

Table 6.1: listing of all the components and their prices

The total price of the multi-tone RF phase modulation is below 2000 USD. This cost is much cheaper than the price of commercial PRBS generators.

Figure 6.2 (left) depicts the intermediate state of the box. And on the right-hand side its final state is shown.

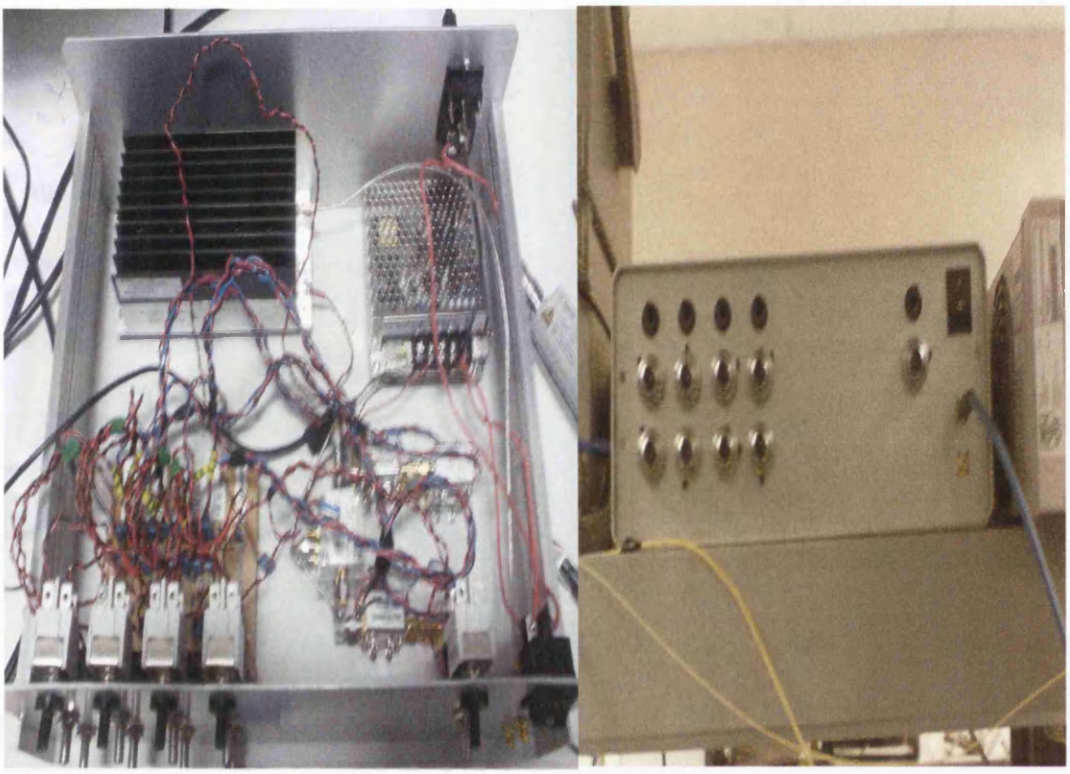

Fig. 6.2 (left) intermediate (right) final state of multi-tone RF phase modulation box.

The other common way for phase-modulating the laser light is PRBS. We did a comparison between the PRBS modulation and Multi-tone modulation in terms of increase in SBS threshold and found that with Multi-tone modulation we can obtain about 3.85 dB in threshold increase over PRBS modulation.

This can also be explained theoretically. As we know the PRBS modulated pump light has a power spectrum of sinc-squared function nature, while with Multi-tone modulation the power spectra can be very flat. We chose the optimum frequencies for the Multi-tone RF modulation by using simulations. We know that if we

modulate the pump by four frequencies f_1, f_2, f_3, and f_4, the pump field is given by the following equation

$$A_p(t) = A_p(0)\exp(i(b_1 \sin(2\pi f_1 t) + b_2 \sin(2\pi f_2 t) + b_3 \sin(2\pi f_3 t) + b_4 \sin(2\pi f_4 t))) \quad [6.5]$$

where b_1, b_2, b_3, and b_4 are modulation indices. We have taken this value as 1.435 for all four RF oscillators. For optimum modulation, the ratio between frequencies should be roughly 3.

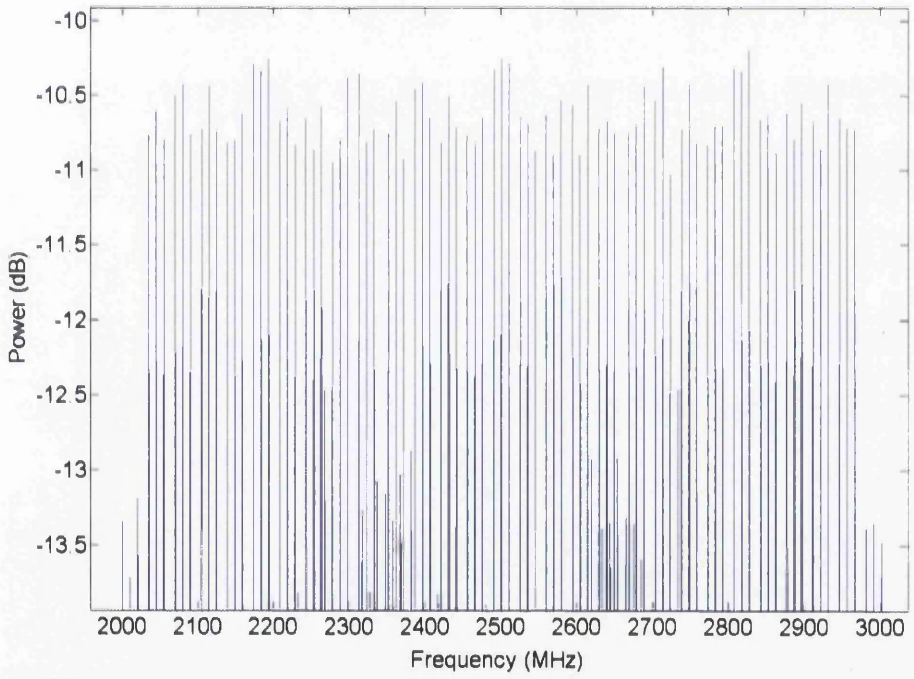

Fig 6.3 Output spectrum due to multi-tone phase modulation

Figure 6.3 shows the simulated output spectrum due to Multi-tone RF modulation, which is very flat, although not exactly flat.

6.4 Experimental Output Spectra due to Multi-tone and PRBS RF modulation

6.4.1 Experimental set-up

Figure 6.4 shows the experimental set-up for measuring the output spectra of both types of phase modulation techniques. We used heterodyne detection to acquire the spectrum of the phase-modulated laser through measuring with an electrical signal analyzer its beating with a CW laser at a slightly different wavelength. We used two tunable laser sources for this, one of which was phase modulated by either Multi-tone or PRBS. Then we mixed them through the 50/50 coupler and obtained beating between the two laser sources. We used a photodetector to obtain the spectrum on the ESA. We also used a polarization controller before the phase modulator, as it is very polarization-sensitive.

The four frequencies for Multi-tone modulation were 100 MHz, 320 MHz, 980 MHz, and 2220 MHz.

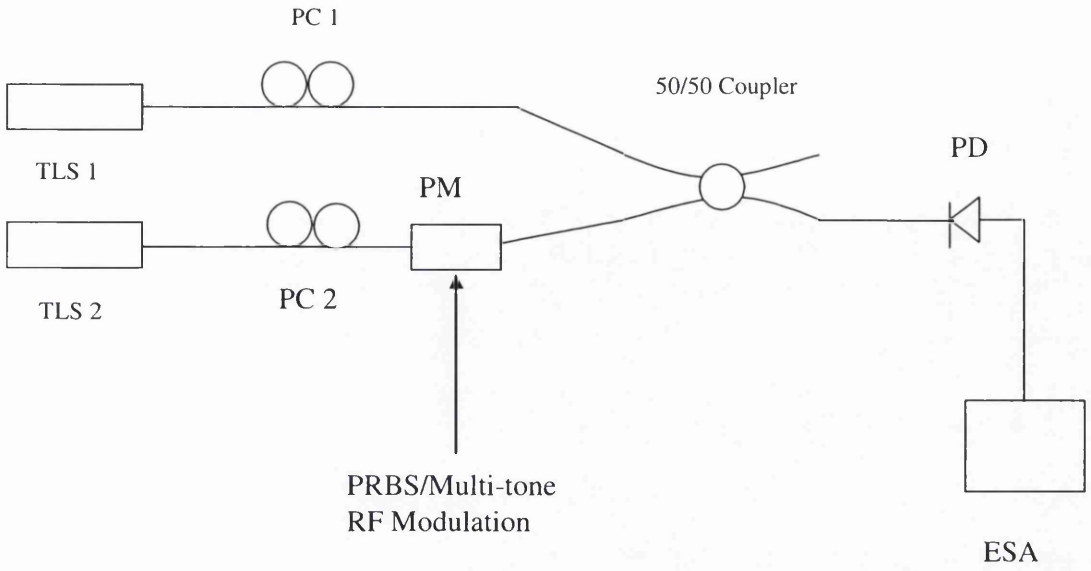

Fig 6.4 Experimental set-up to measure the pump spectra due to phase modulation by either type of technique

6.4.2 Experimental Spectra

The results are depicted in Fig. 6.5. It shows the optical spectra of the laser after modulation by a 2.5 Gb/s PRBS, and a multi-tone signal with four frequencies ranging from 50 MHz to 2.6 GHz. We note that the spectrum for multi-tone is more uniform than that for PRBS. This is beneficial, as it indicates a better utilization of the RF power

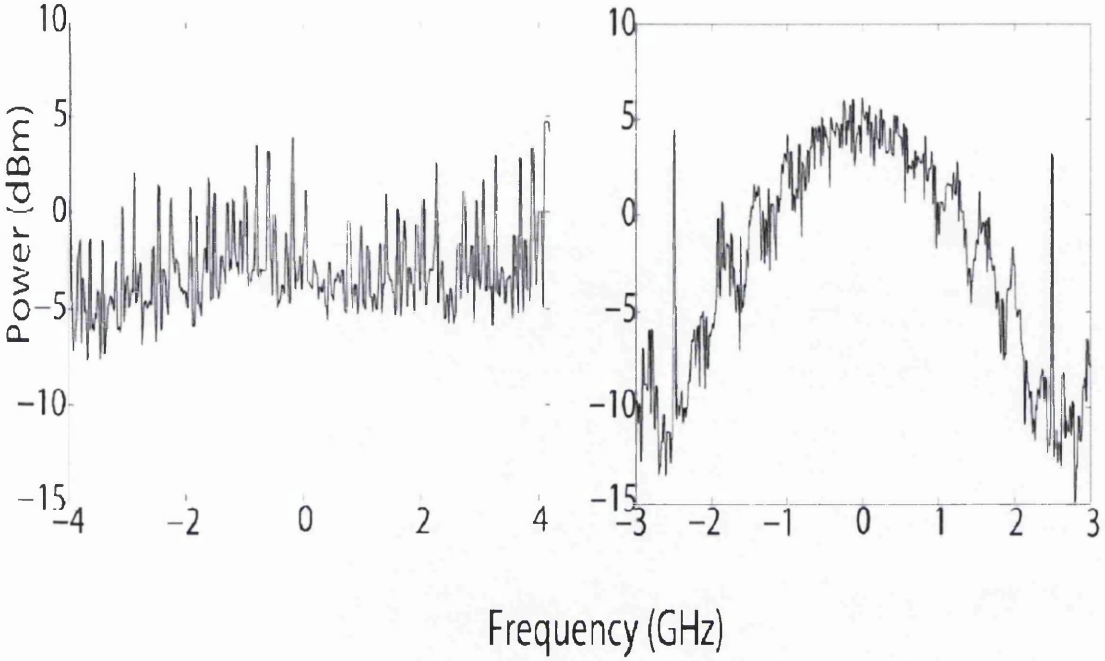

Fig 6.5 Optical power spectra for RF phase modulation by multi-tone (left) and PRBS (right)

6. 5 Threshold Measurements

6.5.1 Experimental Set-up

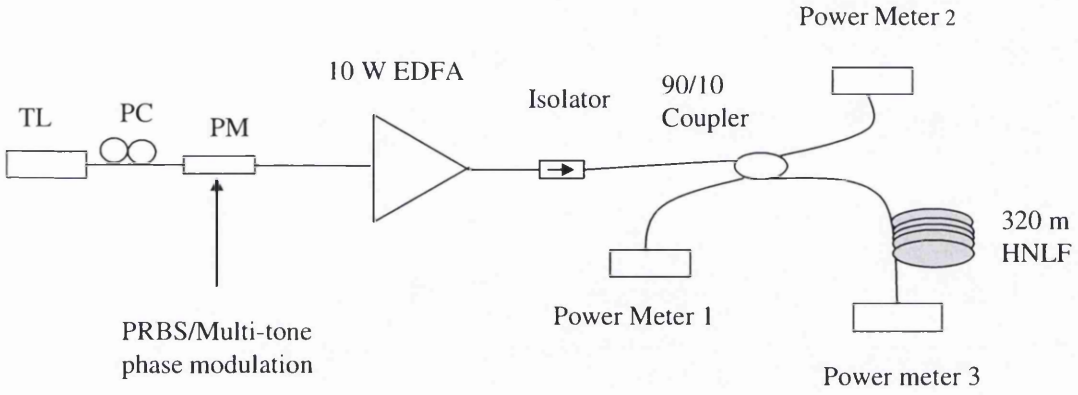

Fig 6.6 Experimental set-up to measure SBS threshold for both techniques

Figure 6.6 shows the experimental set-up for measuring the SBS threshold. Light from the tunable laser source goes to the polarization controller, and then to the phase modulator, which is driven by the PRBS or Multi-tone modulation separately. Then it goes to the 10 W EDFA, then to the isolator, which prevents back reflected light going into EDFA. Then it goes into one port of the 90/10 coupler. Power meter 1 measures the back reflected light, while power meter 2 measures the input light; power meter 3 measures the light transmitted through the fiber. We also did loss calibration, which we incorporated into our readings later. We plotted the curve between input and reflected light, input and transmitted light for: no phase modulation; with PRBS RF phase modulation; and with Multi-tone RF phase modulation.

6.5.2 Results

Figure 6.7 shows the reflected power versus input power graph. If we define the SBS threshold as the input power where the back reflected light start to increase in a non-linear manner, then the SBS threshold without any phase modulation is 40 mW. With PRBS modulation technique this goes up to 0.7 W, while with multi-tone RF modulation scheme it further goes up to 1.6 W. This shows an improvement of 3.6 dB in SBS threshold over PRBS, and an overall increase of 16 dB over no phase modulation. From this we can conclude that our multi-tone RF modulation technique is better than the PRBS modulation technique in terms of enhancement in SBS threshold. And, in earlier work people have shown that multi-tone RF modulation is better even in terms of SNR penalty. [6.7]

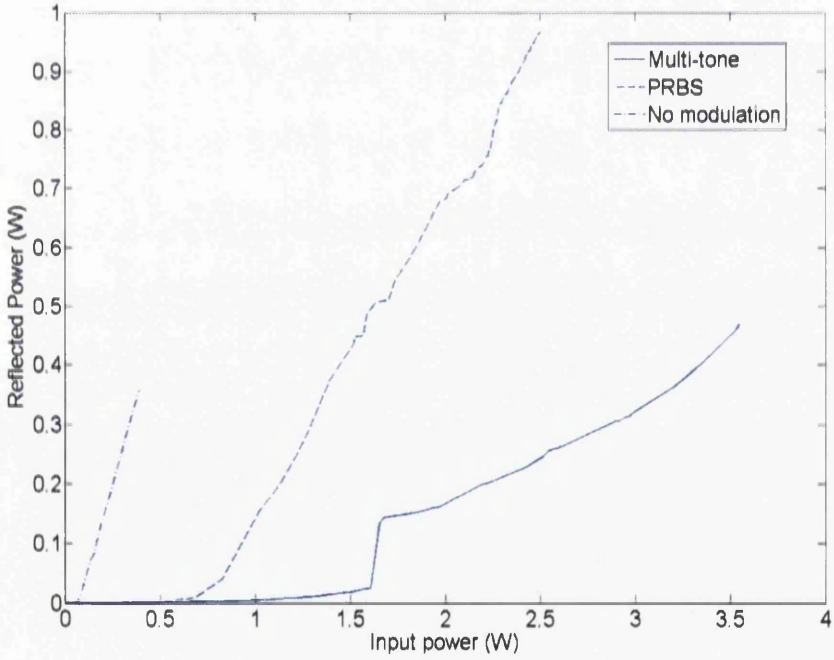

Fig 6.7: Reflected power versus input power

Figure 6.8 plots the transmitted light vs. the input power launched. It is clear that with multi-tone RF phase modulation we were able to transmit more light, in comparison to that of 3 Gb/s PRBS phase modulation

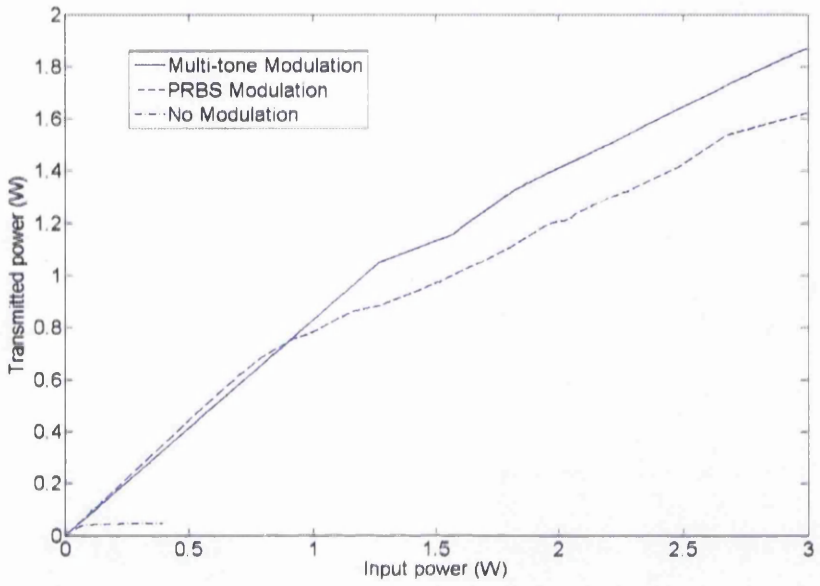

Fig 6.8: Transmitted power versus input power

6.6 Conclusion

We have experimentally compared PRBS and multi-tone phase modulation. We showed that the latter enables a further improvement of 4.18 dB in SBS threshold, which is helpful for applications using high power CW pumps in optical fibers and is less expensive to implement.

References

6.1 Robert W. Boyd, "Nonlinear Optics", second edition, Academic Press, San Diego, USA, 2003

6.2 Govind P Agrawal, "Nonlinear Fiber Optics", fourth edition, Academic Press, San Diego, USA, 2007.

6.3 J.D. Marconi, J.M. Chavez Boggio and H.L. Fragnito, "Narrow linewidth fibre-optical wavelengthconverter with strain suppression of SBS, *Electron. Lett.*, vol. 40, p. 1213, 2004.

6.4 J. Hansryd, F. Dross, M. Westlund, P. A. Andrekson, and S. N. Knudsen, "Increase of the SBS Threshold in a Short Highly Nonlinear Fiber by Applying a Temperature Distribution", *J. light-wave technol.*, vol. 19, p. 1691, 2001.

6.5 Y. Aoki, K. Tajma, and I. Mito, "Input Power Limits of Single- Mode Optical Fibers due to Stimulated Brillouin Scattering in Optical Communication Systems", *J. Light-wave Technol.*, vol. 6, p. 710, 1988.

6.6 S. K. Korotky, P. B. Hansen, L. Eskildsen, and J. J. Veselka, "Efficient Phase Modulation Scheme for Suppressing Stimulated Brillouin Scattering," in

Tech. Dig. Int. Conf. Integrated Optics and Optical Fiber Comm., vol. 1, paper WD2–1, pp. 110–111, Hong Kong, 1995.

6.7 A. Durecu-Legrand, A. Mussot, C. Simonneau, D. Bayart, T. Sylvestre, E. Lantz and H. Maillotte, "Impact of pump phase modulation on system performance of fibre-optical parametric amplifiers", *Electron. Lett.* vol. 41, p. 350, 2005.

Chapter 7

Conclusion

In this thesis we have investigated several applications of continuous-wave (CW) fiber OPAs, exploiting the properties of silica-germania highly-nonlinear fibers, as well as the availability of high-power CW pumps in the C- and L-band.

We first studied the potential application of fiber OPAs to agile all-photonic network systems. From the experimental data we showed that their gain needs to be controlled under the varying input conditions. We have shown by experimental data that all-optical gain control (AOGC) works very well in controlling the OPA gain. AOGC avoids saturation, and flattens the gain spectrum, which are two requirements for amplifiers used in WDM amplification. We reduced signal gain variation down to 0.5 dB, for input signal power varying from -25 dBm to -5 dBm. Cross gain modulation was improved from 3 dB to below 0.5 dB. We have also shown from the experimental data that power penalties at BER of 10^{-8} are also improved from 2.5 dB to 0.5 dB.

In future work a better modulation format for fiber OPAs, such as RZ DPSK, in conjunction with AOGC can be used to improve the functionality of fiber OPA even more.

We then exploited the large bandwidth and gain of fiber OPAs to make OPOs with high output power. First we used a fiber OPO with pump wavelength around 1561 nm. This gave us 211 nm of tuning range, and watt-level output power from 1600 nm to 1670 nm. We then we measured the OPO output linewidth, with an OSA at its highest resolution (0.06 nm), and deconvolving its resolution. We also measured the linewidth by heterodyne detection. By both methods, signal and idler

linewidths were measured to be 0.08, and 0.15 nm respectively. This kind of narrow linewidth and high output power source can be very useful for nonlinear applications, optical communication, Raman pumping, gas detection, etc.

We then switched to a different HNLF with a longer ZDWL. With it we made another fiber OPO, and we obtained the largest tuning range for a CW fiber OPO that has been achieved so far, to the best of our knowledge. Also, when the output coupling fraction was increased, we obtained large output powers (20-25 dBm) from 1610 nm to 1720 nm. Laser sources with this much output power and in this wavelength region are very rare. Such sources could potentially find applications in remote sensing, Raman pumping or seeding, and other nonlinear applications.

We then used the large output power of the previous OPO to make another source with very high output in U-band. This was a Raman amplifier, seeded by the output of our tunable OPO, and pump by a strong C-band pump. The gain medium was 2 km of OFS Raman fiber. This gave us more than 3-W of output power in the U-band. A Raman pump power of only 3 W was used, and we obtained nearly 100% conversion efficiency. Again such a powerful light source can be very useful for the above-mentioned applications.

One problem with launching such high CW powers into fibers is back-reflected light, particularly that due to SBS. Phase dithering of the pump is a very commonly used technique to increase the threshold for SBS. We built a multi-tone RF phase modulator, and compared its performance to that of PRBS method, in terms of SBS threshold and cost. We saw an improvement of 4.18 dB in SBS threshold over PRBS. And the cost of this approach much lower than that for PRBS.

In this thesis, we have made significant progress on different fronts in the application of nonlinear fibers and high-power CW pumps to fiber OPAs and OPOs, in photonics networks and to produce high power sources respectively. The CW high power term, mentioned in this thesis is limited to about 10 W. The reasons for limitation are the cost of making such high power sources, absence of optical components which can take such high powers and back reflecting light, mainly SBS. However, in principle it is possible to envision extending this work to much higher powers, as the necessary components become available, and making HNLFs that increase the SBS threshold . Also, with methods to shift the ZDWL of the HNLF, it is possible to extend the range of the output sources through fiber OPOs. For example we know that single-mode fiber lasers and amplifiers can generate as much as 10 kW CW near 1 μm and much less than that at 1550 nm. For instance IPG launched such a laser in 2009. It is thus legitimate to ask whether it will eventually be possible to make fiber OPOs that can use pumps with this kind of power. If this became feasible, one could contemplate the operation of tunable CW OPOs with output power in the kilowatt range, and possibly tunable over hundreds of nanonmeters. It seems that there is no fundamental physical limitation to doing this. However, there are severe practical constraints. The first one is SBS, as in all high-power CW systems. The other one is that all the components used in such an OPO would have to withstand kilowatt-level powers; most of these components do not presently exist, and would have to be developed from scratch. In that respect, it seems that part of the system should probably use free-space components, as these could have a better chance of withstanding such high powers, compared to all-fiber devices. Making such components should in principle be feasible, although it will not be cheap to do it. So, as usual, what will limit the extension of this work to much

higher power levels is economics, and the emergence of applications that would require such high-power OPOs. Hence, while it is clear that the development of higher-power fiber OPOs will continue, it is difficult to estimate at this time the speed at which this will take place.